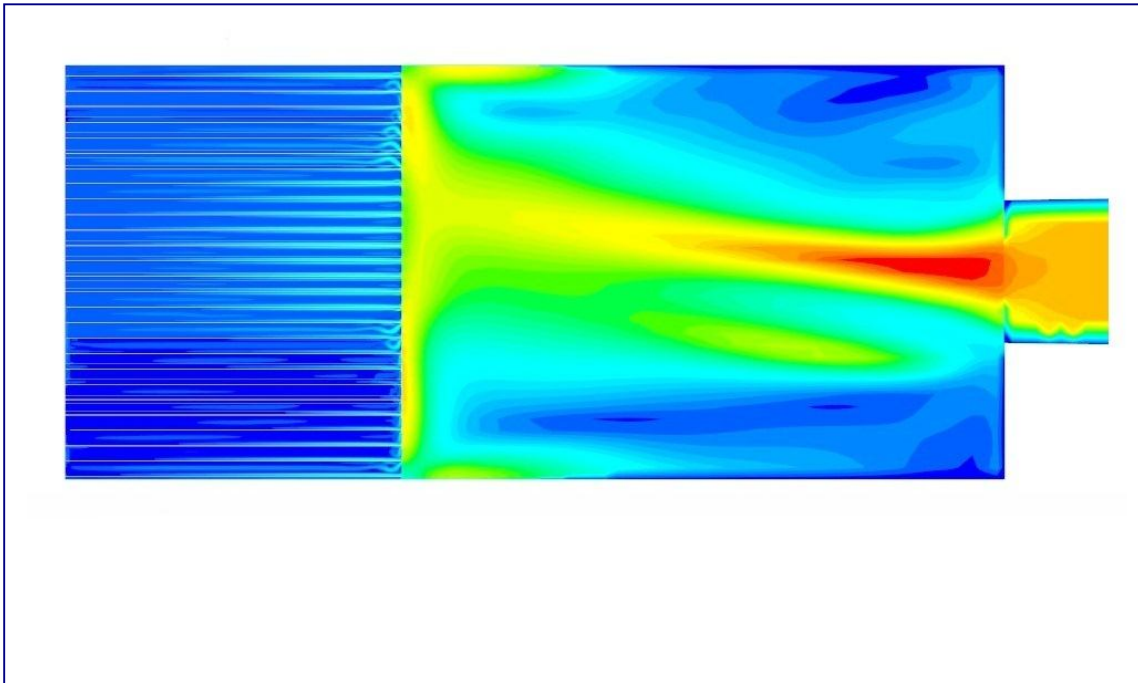# CHALMERS

CFD and Experimental Analysis of Diesel Particulate Filter

Master's Thesis in the Solid and Fluid Mechanics

ELNAZ SAMEI

Department of Applied Mechanics
Division of Fluid Dynamic
CHALMERS UNIVERSITY OF TECHNOLOGY
Göteborg, Sweden 2012
Master's thesis 2012:57

MASTER'S THESIS IN SOLID AND FLUID MECHANICS

CFD and Experimental Analysis of Diesel Particulate Filter

ELNAZ SAMEI

Department of Applied Mechanics
Division of Fluid Dynamic

CHALMERS UNIVERSITY OF TECHNOLOGY

Göteborg, Sweden 2012

CFD and Experimental Analysis of Diesel Particulate Filter

ELNAZ SAMEI

Cover:
The plane cut through the inlet channel and filter box of the Mistra diesel particulate
filter

CFD and Experimental Analysis of the Diesel Particulate Filter

Master's Thesis in the *Master's of Solid and Fluid Mechanics*
ELNAZ SAMEI
Department of Applied Mechanics
Division of Fluid Dynamic
Chalmers University of Technology

ABSTRACT

The diesel particulate filter (DPF) is a device designed to remove diesel particulate matter or soot from the exhaust gas of a diesel engine. The DPF is often used in combination with other exhaust after treatment devises, such as DOC (diesel oxidation catalyst) or SCR (selective catalyst reduction) in order to clean the exhaust gases before emission to the atmosphere.

A DPF system based on sintered metal sheets has been developed in a previous research project at Volvo GTT. A series of tests have been performed on a down scaled DPF prototype. This prototype had high filtration efficiency. Then the next step is to study the soot and ash handling capacity of DPF system and perform tests on a full-scale prototype. In order to move forward to the next step the functionality of the filter should be investigated. Moreover, a complete model of flow inside the filter can help parameter investigation on both downscale and full-scale prototype.

This master thesis aims to study the design and functionality and pressure drop prediction of the DPF in terms of soot accumulation by simulation of flow pattern inside the filter using a CFD tool. Building up a CFD model using StarCCM+ which is capable to simulate the flow through all channels and porous media of the filter plates and tuning the pressure drop parameters for all steps of filtration from clean filter to dirty one are the main achievements of this project. CFD results have been tuned by using experimental data of filtration tests.

Key words: CFD, filtration, pressure drop, diesel particulate filter (DFP), soot accumulation

ACKNOWLEDGEMENT

Preface

In this study CFD analysis has been done for the Mistra DPF prototype at Volvo Group Truck Technology (GTT). The project is a part of the E4 Mistra project which is focused on low emission exhaust. The project approach is to apply advanced systems including catalysts and filter substrates. This master thesis is aimed to study the functionality of the designed filter substrate by CFD simulation.

The thesis project is carried out in cooperation with Applied Mechanic departments (Fluid Division) at Chalmers University of Technology and Volvo Group Truck Technology Advance technology and research and is financially supported by Volvo GTT. The project has been done under the supervision of Professor Lars Davidson from Applied Mechanics Department at Chalmers and co-supervision of Lennart Lundqvist at Volvo GTT. All tests have been done in the laboratory of Volvo GTT advance technology and research center at Chalmers Science Park.

The thesis report includes four chapters. The first chapter is dedicated to problem definition, background, theory and previous work on this subject. Second chapter explains the method of the model simulation and consists of explanation of model geometry, mesh generation and solver properties. In third chapter results of the simulation are presented and discussed. Last chapter includes conclusion and outlook of future work.

Göteborg, Jun 2012

Elnaz Samei

NOTATION

v_i	velocity in x direction
v_j	velocity in y direction
v_k	velocity in z direction
t	time
μ	dynamic viscosity
$\acute{v}$	Fluctuation velocity
k	kineic energy
ε	dissipation
$\bar{v}$	averaged velocity
P^k	production term in kinetic energy equation
ρ	Kinematic viscosity
ν	Density
ν_t	turbulent viscosity
σ_k	adjustable dimensionless parameter in $k - \varepsilon$ model equation
σ_ε	adjustable dimensionless parameter in $k - \varepsilon$ model equation
$C_{\varepsilon 1}$	adjustable dimensionless parameter in $k - \varepsilon$ model equation
$C_{\varepsilon 2}$	adjustable dimensionless parameter in $k - \varepsilon$ model equation
C_μ	constant parameter in expression of turbulent viscosity
y^+	normalized wall distance
k_p	permeability factor
β	parameter in Forchheimer equation
f_P	porous source term in momentum equation
P	porous resistance tensor
P_v	viscouse resistance tensor

Contents

II

1   Introduction

1.1   Background

Diesel particulate filters (DPF) are devices which mechanically prevent the emission of exhaust gas pollution to the atmosphere. These devices have been developed to exceed the efficiency up to the 90% and simultaneously they have a good enough mechanical and thermal stability [1].The main concern of DPF application is the reduction of pollutants emitted by diesel engines in the heavy duty vehicles. Among all pollutant of the fossil fuel engines, like carbon monoxide, various types of hydrocarbons and nitrogen oxide which all are poisonous and harmful for environment, particulate matter is one of the main concerns. It is estimated that one hundred thousand people die prematurely every year due to particulate matter only in Europe [2].

Therefore particulate emission standard has been adopted by authorities in EU, United State and Japan since early 2000 [1].

Some of important standards for diesel emission vehicle in transport sector are [1]:

Heavy –Duty Engines:

-JP 2005, PM=0.0027 g/kWh

-US 2007, PM=0.01 g/bhp-hr

-Euro VI 2013, PM=0.01 g/kWh

Balk density of diesel particulates is typically lower than 0.1 gr/cm^3 so DPF filters accumulate large amount of soot in a short period of time. Possibly several liters of soot per day can be collected in an old heavy-duty truck [2].This high load of soot causes drastic pressure drop for exhaust flow while passing through the DPF filter. Therefore, prediction of the pressure drop is one of the important factors in design and application of DPF. Moreover, pressure drop due to blockage of filter points out the necessity of regeneration of filter. Regeneration of the DPF can be performed continuously during operation of filter or occasionally when a special amount of soot has accumulated in the filter [1].

Various types of filters are the wall-flow (DPF), flow through (FTF) and monolithic reactor. A monolithic catalyst reactor is made of porous material as a cylinder which constitutes many small parallel channels running in the axial direction. The porous media is typically made of ceramic and the wash coat (deposited catalytic material over monolith channels) is applied to maximize the available surface area of filtration. Catalytic filtration is usually used to oxidize gaseous pollutant [1].

Wall flow diesel particulate filters (DPF) are one of the most effective types of particulate filters especially in diesel application. In this type of filter, channels are alternatively plugged at the end. This construction makes the flow pass through the filter plates which are located at the top and bottom of each channel. In other words, flow only enters the channels which are open to the inlet side and only exits the channels which are connected to the outlet side. During the filtration process, by accumulation of soot inside and over the porous media of the filter plates, the efficiency will increase up to 90%. Deposition of soot in DPF is normally a physical absorption process but there are types of DPF which are coated by catalysts [1, 2].

Flow Through Filters (FTF) is exactly designed as a monolithic reactor but the idea is to decrease the particulate load of the flow. In order to achieve this aim, a DOC (diesel oxidation catalyst) in the form of a reactor is located upstream of FTF. The DOC can reduce the particulate matter content by generating NO_2. The trapping efficiency of FTF is generally lower than DPF [2]. The gas flow in wall flow filter is forced to pass the filter plates since every second channel is blocked at the end. So, the gas passage through the wall results in higher trapping efficiency for DPFs.

Among these three types, wall-flow filters are the most effective ones due to high filtration efficiency, lower pressure drop and good regeneration characteristics [3]. Moreover, main research efforts have been concentrated on this type of filters due to good balance between drawbacks and advantages [4].

In many areas of engine and combustion research, application of numeric and computational tools has been developed instead of expensive pilot-scale research models. Moreover, complementing data from prototype demands simulation which allows comprehensive investigation of flow and physics phenomena [2, 4].

The present thesis introduces and discusses a CFD model of the diesel particulate filter, based on a designed prototype for E4 Mistra research project at Volvo Technology AB. The main focus is on analyzing the flow through the filter system and prediction of pressure drop. The flow has been simulated mono phase.

Thesis objectives are:

-   Simulation of flow field in a deposit particulate filter
-   Prediction of pressure drop in different steps from clean filter to dirty filter
-   Tuning the viscous resistance factor in the pressure drop equation for porous media
-   To investigate the design efficiency of Mistra DPF
-   To investigate the possibility of soot-build up simulation and soot distribution over filter plate in Mistra DPF using StarCCM+

1.2   Previous Work

DPF simulation has been investigated from different aspects. In this chapter some of these aspects are reviewed briefly.

A.J. Torregrosa et al. [4] presented a wall-flow DPF model which is integrated into a gas dynamic code for internal combustion. They considered one dimension unsteady compressible flow for monolith filter and made a radial discretization of the cross section of channels. The partial differential equations generated of this model include a source term for considering loss or gain of flow through the porous walls. The description has covered the geometrical and mathematical representation of the DPF system, with emphasis on fluid dynamic aspects. Moreover, they have discussed the possibilities for simple extension to filtration and regeneration analysis. The model showed good agreement with experimental result for example proper distribution of pressure drop across the monolith. The specific analysis of the pressure and velocity fields in monolith channels was also shown [4].

P. Tandon et.al. [3] studied a theoretical and experimental method to explain the sensitivity of filtration behavior on filter properties. A laboratory setup is described to

measure evolution of mass based filtration efficiency. In order to describe the impact of various testing parameters on filtration behavior, a dynamic soot loading model is also presented that accounts for different soot particle capture mechanisms. The method presented in this paper is focused on microstructure filtration and is able to capture the soot deposition behavior and soot absorption inside the DPF wall by Brownian diffusion, particle interception and particle inertia [3]. The results have shown that clean filter efficiency (FE) is rather insensitive to the wall filter porosity but it is very sensitive to wall pore size. FE decreases by increasing median pore diameter. While clean FE increases by decreasing wall median pore size, a significant increase in clean filter pressure drop is observed for wall median pore diameter below 10-12 µm. If two filters have the same pore size, the one which has larger wall thickness exhibits higher clean FE. Filtration behavior of the same filters in two different temperatures (room temperature and 300 C) showed FE is higher in higher temperature [3].

H. Ström et.al. [5] investigated Eulerian-Lagrangian CFD modeling to track eight types of typical diesel and gasoline soot particles through a flow–through substrate with protrusions. It is shown that there exists a minimum trapping efficiency for medium-size soot particles ($dp = 150$ µm). The computational mesh domain represents a part of substrate. The substrate size is 4.00×1.05×6.00 mm. The height of the channel is 1 mm and the sine wave-like wall structures inside the domain have a thickness of 50 µm [5].

In Eulerian-Lagrangian modeling, particle motion in the system will be determined by the net effect of the different forces acting on the particles. The most important forces in aerosol systems which are considered in Ström's work are drag and lift forces, gravity force and Brownian motion. Some results presented by this paper are as below [5].

- There exists a minimum trapping efficiency for medium-sized soot particles in this device,
- The dominating particle trapping mechanisms are Brownian diffusion and inertial impaction,
- Different types of particles are trapped by different mechanisms. The smallest particles are affected by Brownian motion whereas the largest particles are conducted by inertial impact.
- Trapping of small particles increases by lower velocities while the trapping of larger particles increases by increasing the velocity.

U. Janoske et. al. [6] work is focused on modeling of the filtration and regeneration based on pressure drop factor. They developed a mathematical model which describes the loading and regeneration behavior of a DPF. The model is integrated in a commercial CFD code using a user defined subroutines (UDS). The CFD code was used for the calculation of the fluid flow and the particle tracks of different kinds of particles in two dimensional model of the DPF. Since non stationary filtration processes with a variable height of the particle surface cannot be simulated using commercial CFD codes, the computation is accomplished by combining a CFD code with self-defined program routines for a 2D computational grid. After computation of the flow and temperature field by CFD code, the particle tracks are calculated using

Euler-Lagrange approach. These data are input information for USD. Knowing the position of the separated particles on the ceramic wall and on the deposits which is already formed, the surface layer height and flow resistance over the DPF can be computed.

Finally, the presented model simulated the behavior of loading the filter, especially pressure drop. The results were in good agreement with experimental data [6].

1.3   Theory

1.3.1   Governing Equations

In this chapter the theory of numerical calculation is discussed. More details about flow theory and calculation can be found in CDF reference text book [7].

The basic idea of the governing equations in a control volume includes three aspects of mass, momentum and energy:

-mass of the flow is conserved

-rate of change of momentum is balanced by the sum of total forces on the control volume

-rate of change of energy is equal to the sum of the rate of heat and work addition to the control volume

Writing the mass, momentum and energy balance differential equations for a 3D control volume and simplifying those equations leads to Navier-Stokes set of equations. Air in low velocities can be considered as incompressible fluid so the governing equations are:

$$\frac{\partial v_i}{\partial x_i} = 0 \tag{1.1}$$

$$\rho \frac{\partial v_i}{\partial t} + \rho \frac{\partial v_i\, v_j}{\partial x_j} = -\frac{\partial p}{\partial x_i} + \frac{\partial}{\partial x_j}\left(\mu \frac{\partial v_i}{\partial x_j}\right) \tag{1.2}$$

In order to describe turbulent flow it is necessary to investigate the mean flow properties and also effects of turbulence on these properties, so the time averaged Navier-Stokes (RANS) is introduced as:

$$\rho \frac{\partial \bar{v_i}}{\partial t} + \rho \frac{\partial \overline{v_j}\,\overline{v_i}}{\partial x_j} = -\frac{\partial \bar{p}}{\partial x_i} + \frac{\partial}{\partial x_j}\left(\mu \frac{\partial \bar{v_i}}{\partial x_j} - \rho \overline{\acute{v_i}\acute{v_j}}\right) \tag{1.3}$$

There is an extra term in RANS equation (1.3) which does not have any exact solution and should be modeled. $k - \varepsilon$ model is one of the best known models for this application. The steady state form of this model [8]:

$$\bar{v_j}\,\frac{\partial k}{\partial x_j} = P^k + \frac{\partial}{\partial x_j}\left[\left(v + \frac{v_t}{\sigma_k}\right)\frac{\partial k}{\partial x_j}\right] - \varepsilon \tag{1.4}$$

$$\bar{v_j}\,\frac{\partial \varepsilon}{\partial x_j} = \frac{\partial}{\partial x_j}\left[\left(v + \frac{v_t}{\sigma_\varepsilon}\right)\frac{\partial \varepsilon}{\partial x_j}\right] + \frac{\varepsilon}{k}\left[c_{\varepsilon 1}P^k - c_{\varepsilon 2}\varepsilon\right] \tag{1.5}$$

$$v_t = c_\mu \frac{k^2}{\varepsilon} \tag{1.6}$$

$$P_k = v_t\left(\frac{\partial \bar{v_i}}{\partial x_j} + \frac{\partial \overline{v_j}}{\partial x_i}\right)\frac{\partial \bar{v_i}}{\partial x_j} \tag{1.7}$$

This set of equations includes five universal constants ($c_\mu, \sigma_k, \sigma_\varepsilon, c_{\varepsilon 1}, c_{\varepsilon 2}$) which are determined by data fitting [8]. The standard $k - \varepsilon$ model employs values in equation (1.8) which fit for a wide range of turbulent flow [7]:

$$c_\mu = 0.09\ \sigma_k = 1.00\ \sigma_\varepsilon = 1.30\ c_{\varepsilon 1} = 1.44\ c_{\varepsilon 2} = 1.92 \tag{1.8}$$

The general idea of this set of equations is:

Rate of change in k or ε + transport of k or ε by convection = transport of k or ε by diffusion+ rate of production of k or ε – rate of destruction of k or ε [7].

1.3.2   Wall function

Wall function is one of the important concepts in industrial CFD calculation. Using wall functions cause reduction in CPU time. Application of wall functions means the boundary layer near a wall is not resolved but the first node of cells in computational domain is located in the log-low region where y+ lies in the range of 30 to 100 (upper limit may change due to the change of Re number).In fully turbulent flow, the flow between the first node and the wall is assumed to be flat plate boundary layer flow. This assumption is satisfied in many cases [8]. The wall function used in this simulation is "All y+ wall treatment". This function is a hybrid treatment for both high and low y+. This method consists of a set of near wall modeling assumptions for each turbulence model. For example the high y+ wall treatment implies the wall function type approach. The low y+ wall treatment is suitable only for low Reynolds number turbulence model in which viscous sub-layer is resolved.

1.3.3   Porous media

In order to predict the pressure drop over a porous media, the relation between pressure drop and superficial velocity and permeability of porous media is introduced as Darcy's Law:

$$-\nabla p = \frac{\mu}{k_p} v \qquad (1.9)$$

In this equation, v is superficial velocity (m.s^{-1}), μ is viscosity (Pa.s), and k_p is permeability factor (m^2). Darcy Law is valid only for creeping flow, but this equation was further developed by Dupuit and Forchheimer as:

$$-\nabla p = \frac{\mu}{k_p} v + \rho \beta v^2 \qquad (1.10)$$

Equation (1.10) is known as Forchheimer equation and is valid for higher range of velocity. The β factor depends on particular flow and medium of interest. It is commonly determined by experiments [9]

For the flow solver porous source term appears in the momentum equation as tensor, so the above equations become (tensor-vector multiplication):

$$f_p = -P.v \qquad (1.11)$$

P is porous resistance tensor and is given by equation (1.12)

$$P = P_v + P_i|v| \qquad (1.12)$$

In this equation P_v and P_i are the viscous (linear) and inertial (quadratic) resistance tensors, respectively [9]. This equation is used to predict pressure drop for porous media in StarCCM+ commercial code.

2   Method

In this chapter the process of preparing the DPF model for simulation is described. CAD model, mesh generation, equations and parameters for the solver are discussed in the following sections. The last part is dedicated to explain the set up and experiments which are used to validate the simulation.

2.1   Geometry of the domain

The DPF's geometry consists of a filter box, two outlet cones located on both sides and one inlet cone located in front of the filter box. Cones are connected to the pipes so inlet and outlet connections are circular. Figure 2.1 shows the configuration of Mistra DPF. Since the configuration is symmetric only one half of the DPF has been modeled. The CAD model is shown in Figure 2.2 .The simulation consists of solving the flow inside the pipes, cones and filter box.
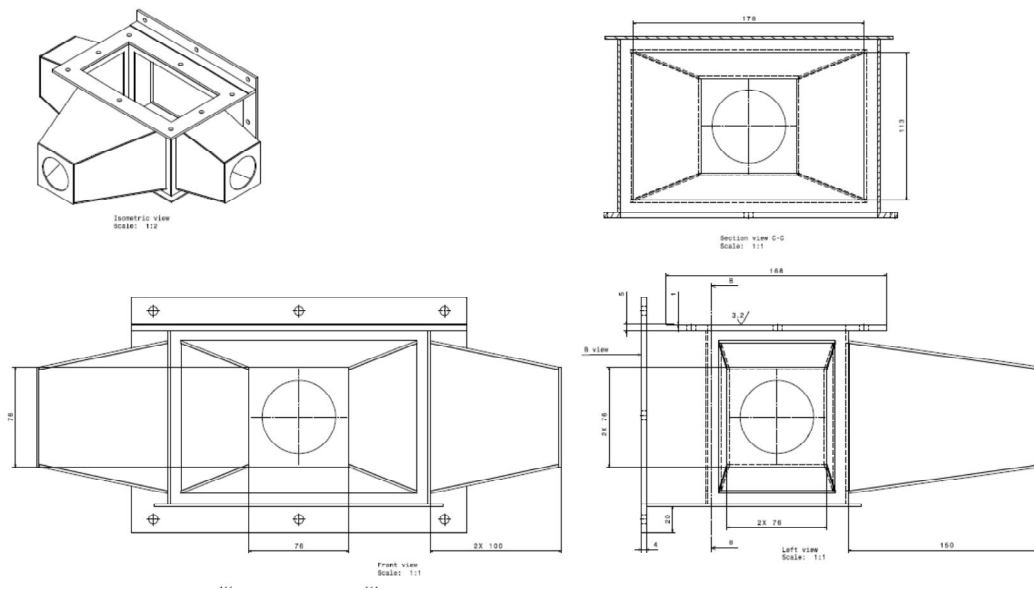
Figure 2.1) Configuration of Mistra DPF
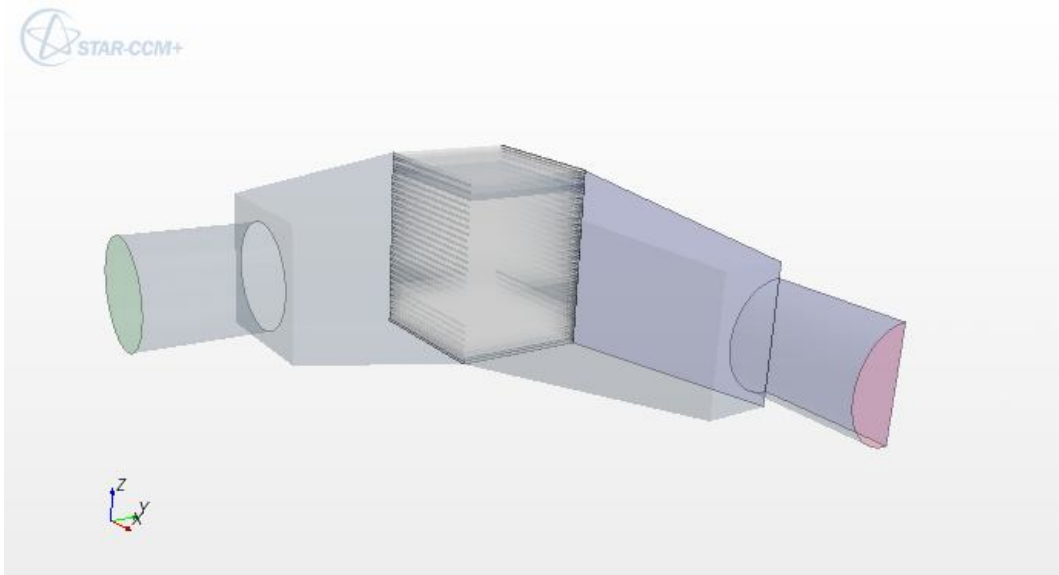
Figure 2.2) CAD model of the DPF

Size of the filter box in the prototype of Mistra DPF is 75✕165✕102 mm. Lengths of the inlet and outlet cones are 150 mm and 100 mm respectively. CAD model is designed exactly based on the prototype.

The filter box consists of 54 porous plates as filters. Each filter plat is surrounded by channels. Inlet channel is located above the filter plate and outlet channel is under it. Therefore the filter box includes 27 inlet channels and 27 outlet channels. As it is described in chapter 1.1, the structure of the DPF is designed in a way that both the inlet and outlet channels are plugged alternatively at the end. Moreover, the inlet channels are only connected to the inlet cone. The same is true for the outlet channels so the flow only enters of the inlet channel and only exits of the outlet channels. This structure lets the flow turn 90 degrees during the filtration process.

To simplify the simulation, the corrugated channels in the prototype were replaced by rectangular channels. Figure 2.3 and 2.4 depict the real and simulated filter box and channels.
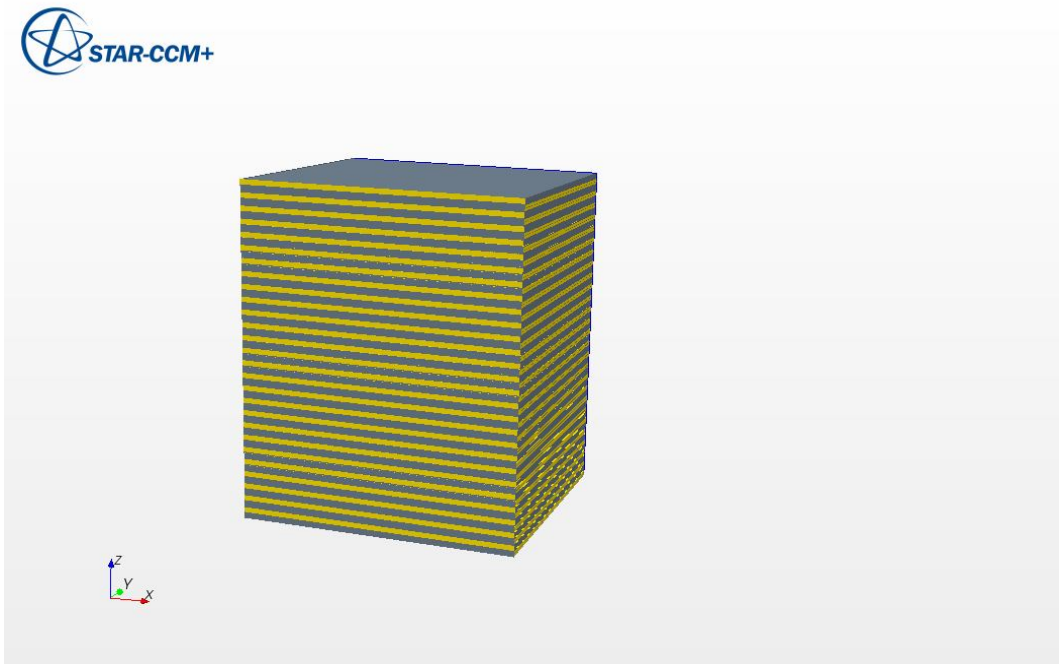

Figure 2.3) Corrugated channels in filter box

Figure 2.4) Filter box CAD model

The height of each channel is 1.5 mm. The filter plate thickness, which is connected to the channel, is 0.35 mm and its porosity and mean pore size, are 0.45 and 10 µm, respectively.

In order to investigate the effect of inlet pipe on the filtration efficiency a CAD model was designed without pipes. In this model the whole front face of the inlet cone is the inlet boundary of the system. Figure 2.5 shows this CAD model.
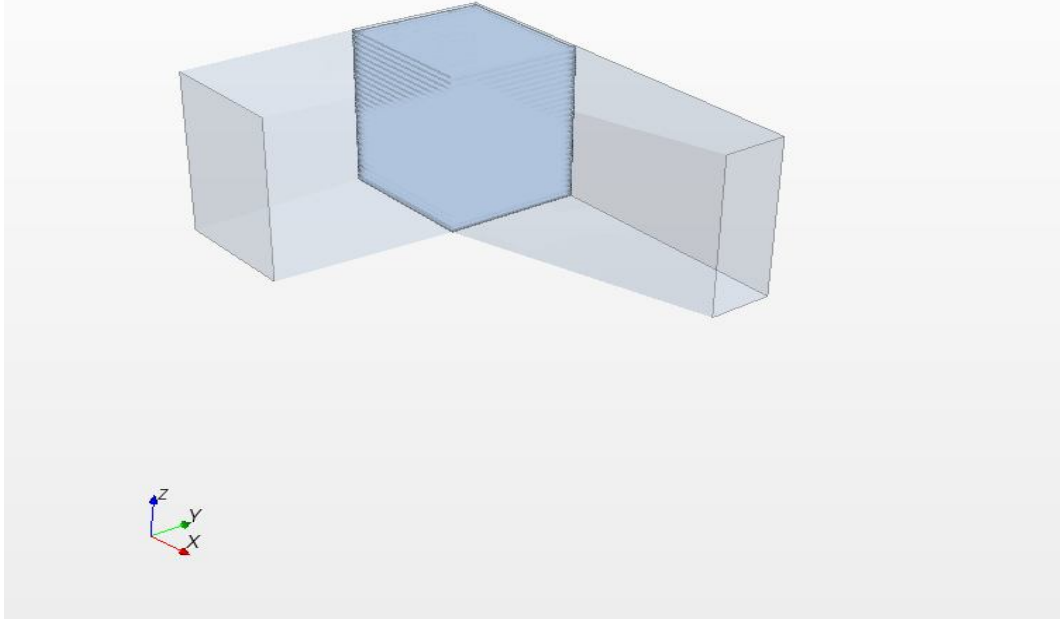
Figure 2.5) CAD model of DPF without pipes

CHALMERS, *Applied Mechanics*, Master's Thesis 2012:57

2.2   Mesh

The mesh generation in Star CCM is divided into two main steps: surface meshing and volume meshing. Surface meshing is the preparation step for volume mesh generation because surfaces generated in CAD model should be closed, manifold, and divided to nearly equal triangles [9]. If quality of the surfaces does not meet the requirement, another step is needed to repair the surface mesh. In this case the surfaces mesh of the CAD model was adequately good to start the volume mesh. The volume mesh model of the system is Trimmed mesh which includes hexahedral cells with minimal skewness. No prism[1] layer was defined for volume mesh inside the filter box but both inlet and outlet cones considered to have two prism layers next to the walls.

As it was explained in previous section, the system is made of different regions and each of them needs different mesh setting. Cones (and tubes) have the base cell size of 3 mm, maximum cell size in this area is 4.5 mm and minimum cell size is 0.75 mm. Channels (both inlet and outlet) have the base cell size of 2mm. An anisotropic mesh model was activated for channels to reduce cell size in Z direction to 0.3 mm. Mesh model for filter region is the same as channels but anisotropic cell size for filters was 0.2 mm. More details of mesh properties in different regions are tabulated in table 2.1.

Table 2.1) Mesh properties for different regions of DPF model

	Cones	**Cones (near entrance and exit of filter box)**	**channels**	**Filters**
Mesh Model	Trimmer	Trimmer	Trimmer	Trimmer
Base size	3 mm	0.51 mm	2 mm	2 mm
Anisotropic mesh	-	-	Z, 0.3 mm	Z, 0.2 mm
Max. cell size	4.5 mm	0.51 mm	2 mm	2 mm
Surface curvature	36 pts/circle	36 pts/circle	36 pts/circle	36 pts/circle
Surface proximity	2 point in gap	2 point in gap	2 point in gap	2 point in gap
Template growth rate	fast	fast	fast	fast

Surface curvature and surface proximity are two parameters which are applied by surface remesher for cell refinement. Growth rate is a property which controls the rate of increasing cell size from one cell to the next one.

---

[1] . A prism layer mesh is composed of orthogonal prismatic cells that usually reside next to wall boundaries in the volume mesh. They are required to accurately simulate the turbulence and heat transfer.

Total number of cells for each CAD model is listed in table 2.2.

Table 2.2) Number of cells in different CAD models

	DPF	**DPF (without pipe)**
Total number of cells	15908752	15904948

Figure 2.6 and 2.7 depict cuts of volume mesh at inlet cone and filter box respectively. Figure 2.8 shows a top view cut of volume mesh.
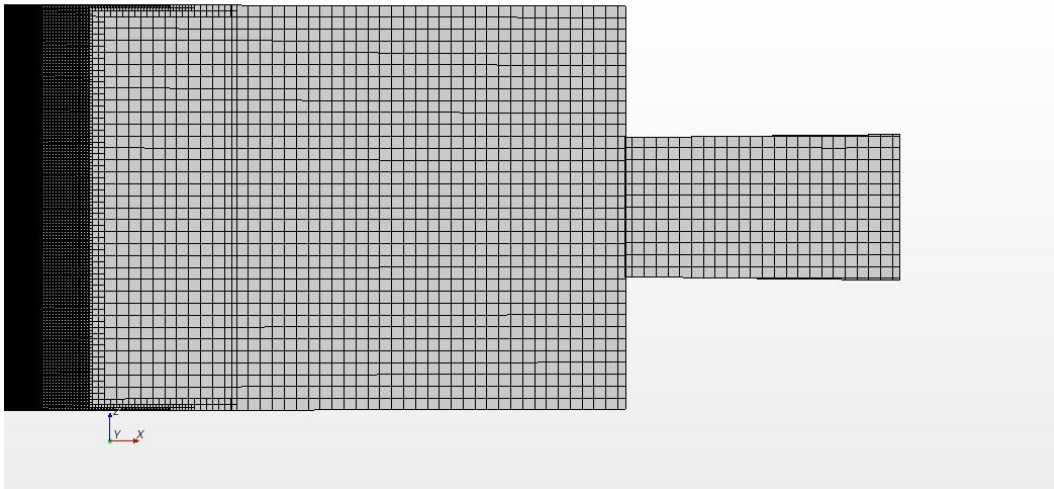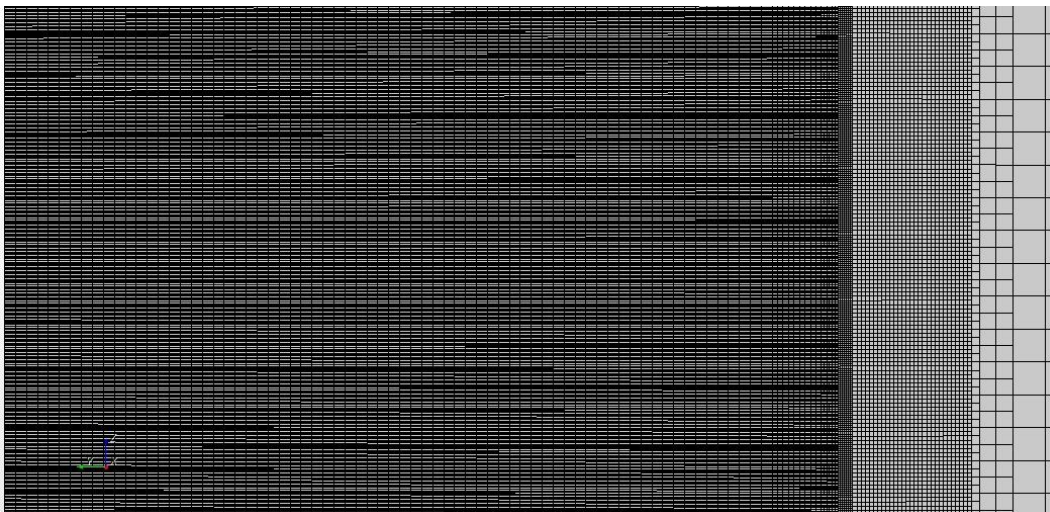

Figure 2.6) Cut of the volume mesh at the inlet cone
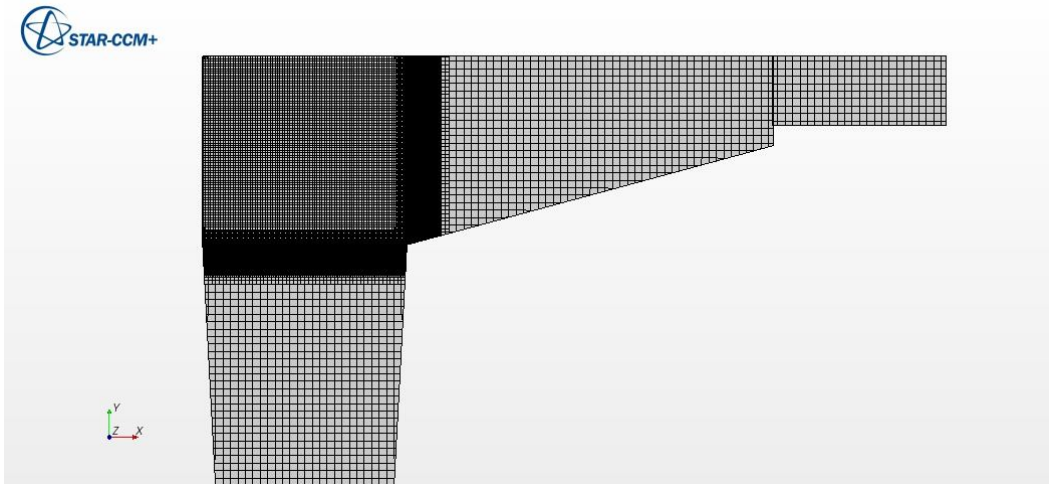

Figure 2.7) Cut of the volume mesh at the filter box

Figure 2.8) Mesh configuration at a cut of top view

The model contains some critical areas the need dense mesh to resolve the flow. The area around the entrance of filter box, inside the inlet cone and also the exit of the flow from filter box to outlet cone are such regions. In order to cover these areas the technique of volumetric control was applied to select these parts of the cones and generate trimmer isotropic mesh with absolute cell size of 0.51 mm.

To make the simulated model of the filter more realistic, the flow inside the inlet channels should be split. In real channels, corrugated plates take this role but in the model simple rectangular channel is replaced the corrugated one. So, this effect is applicable by splitting inlet channels by a row of cells in the middle of the channel. These rows of cells are grouped in a new set of regions called solid continuum and flow is not solved inside them. These regions act as walls. Mesh configuration zoom-in view in Figure 2.9 shows these regions.
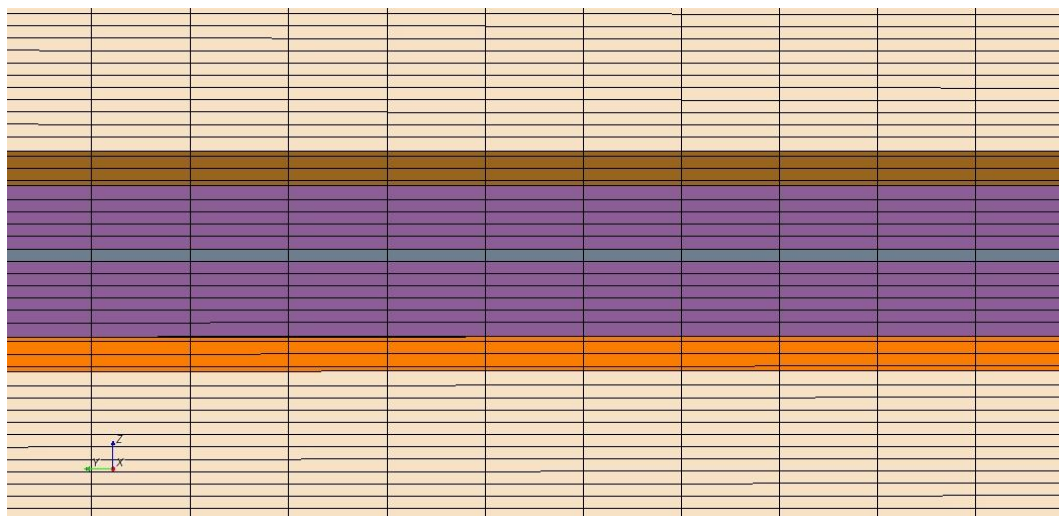

Figure 2.9) Zoom-in view of volume mesh inside the filter box: outlet channel, first filter plate, inlet channel, splitting wall, second filter plate and outlet channel

2.3   Solver

In order to solve the model all the interfaces and boundaries should be defined properly. The model has a symmetry boundary along the symmetry line of the filter box and inlet cone. Inlet boundary is mass flow inlet. The mass flow rate of 1500 rpm engine speed, 50% load, is 37.8 gr/s at the inlet of Mistra filter. This value is set as inlet boundary mass flow of the model. The outlet boundary is ''split mass flow ratio'' which means the inlet mass flow is equal to the outlet mass flow. This is a correct assumption since the flow has been solved mono phase (without soot) for this simulation. Moreover, experiments showed no significant change in mass flow of the inlet and outlet. The only difference between first and second CAD model of DPF (with pipe and without pipe) is the area of inlet boundary. All walls in these two models are no-slip walls.

All models consist of three different types of interfaces: inlet channel/inlet cone, outlet channel/outlet cone, filter plate/channel. The inlet channel/outlet cone and outlet channel/inlet cone interfaces are blocked.

Various types of regions in the model are applied to describe the flow behavior as correct as possible. Both inlet and outlet cones were defined as flow regions. Channels and filters both considered as porous media. Porous media for channels is used to control the flow direction inside this region. The porosity of this region is set equal to 1 but pressure drop coefficients are defined to direct the flow on correct direction. For instance, inside the inlet channels, corrugated shapes conduct the flow in X direction. In simulated model this behavior is simulated by setting high pressure coefficient in Y direction (Figure 2.2). The opposite situation is valid for the outlet channels so in this case pressure coefficient tensor is increased in X direction.

The porous region for filter plates has the porosity of 0.45. The pressure drop coefficient is adjustable parameter to predict the pressure drop of the whole system.

As it is mentioned in previous section, the solid region is introduced inside the inlet channel to let the flow split and pass both the upper and lower filter plates of a neighboring inlet channel. Flow is not solved in this region.

The filtration process is isothermal; therefore, flow is not solved for energy equation. The solver model is segregated. This solver is controlled by under relaxation factor. The matrix solver method is algebraic multi grid parameters [2] (AMT) [9]. Under relaxation factor for different terms are listed in table 2.3.

---

[2] The algebraic multi grid methods solve the discrete linear system iteratively. The AMG Linear Solver node is not as costly as direct methods like Gauss elimination.

Table 2.3) Under relaxation factors

	Under relaxation factor
Velocity	0.7
pressure	0.3
K- ε turbulence viscosity	0.8

The method which is used for wall treatment in StarCCM is ''All y+ Wall treatment'' which is a hybrid treatment for both high and low y+. The details are explained in Section 1.3.2.

2.4   Experiments

2.4.1   Experiment set up

The development and employment of a DPF soot and ash loading method was constructed using a portable power generating set (DX 6000 TE XL C) equipped with Yanmar L100 engine to generate the soot and ash containing exhaust gases. The gen-set configuration and general properties of the system is shown in Figure 2.10. This engine was selected because of its small size, relatively low cost and simple design compared to full-size engine.

The DPF tested in this study was the uncoated prototype, which is a cross flow filter made of flat porous metal powder sheets as filter plates and a corrugated solid metal sheet as flow channels. The porous and corrugated sheets are stacked together. Every second corrugated sheets is rotated 90° to make outlet channel. As it is mentioned in previous chapter system has one inlet and two outlets. Figure 2.11 shows the design of DPF prototype and filter holder.

DX 6000 TE XL C - Generating set

DX 6000 TE XL C Portable Power Generating set, equipped with Yanmar engine.

General characteristics

Max. power (kW)	5.0
Engine trademark / Engine type	Yanmar / L100
Autonomy (h)	9
Noise level dB(A) - 7m	78
Oil Guard	Yes
Start	Electrique
Lenght (cm) x Width (cm) x Height (cm)	87 x 57 x 56
Dry Weight (kgs)	106

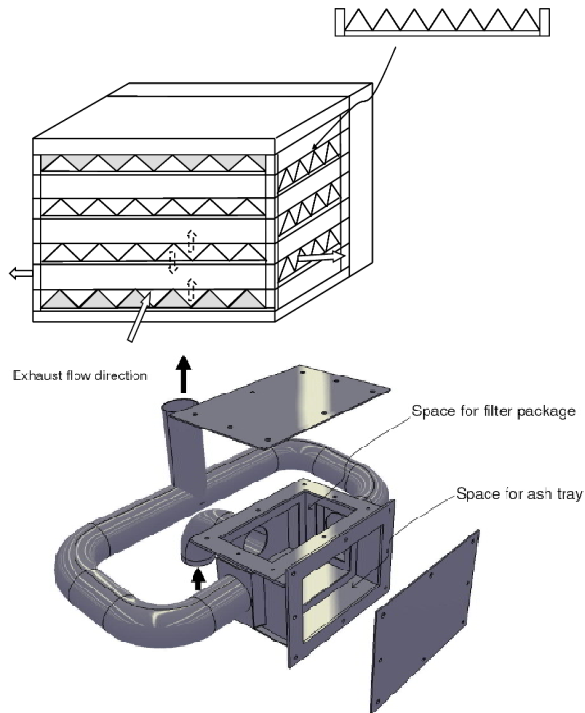*Figure.2.10) Configuration and properties of the DX 6000 TE XL C gen-set [10]*

Figure 2.11): The DPF prototype design (left) and the DPF holder (right) [10]

The exhaust gas was analyzed using a DMS 500 fast particle analyzer to measure the number and size distribution of the particles in the exhaust gas and an MKS FTIR instrument to measure H_2O, CO, CO_2, diesel and NOx.

2.4.2   Accelerated ash loading experiment

The ash storage in the DPF was accelerated in by blending the engine fuel (Volvo standard diesel) with 5 wt. % lube oil (Mobil Delvac XHP Extra 10W-40) which contains 1.9 wt. % sulfated Ash (ASTM D 874). At start-up the engine was run on pure diesel in idling mode until steady state conditions was achieved. Then the load was increased to 4 kW and after a few minutes, when steady state conditions was achieved, the fuel supply was switched to the tank with lube oil blended diesel to start the accelerated ash storage.

 During the ash and soot storage step, the pressure drop gradually increased. When the pressure drop reached 45 mbar the DPF has been packed with soot and ash and it is ready to be regenerated.

3 Results

In this section results of the experiment and CFD simulation are analyzed. The objective of experiments is to tune the pressure drop coefficient by comparing the CFD results with experimental data. In the following section experimental data are described and in section 3.2 CFD simulation results of the flow field and pressure distribution are discussed. Section 3.3 is dedicated to investigate the efficiency of Mistra DPF structure by comparing DFP and DPF without pipe models. In section 3.3, two samples of the simulation residuals are depicted.

3.1.1 Experimental data

The experiments have been done in quite the same mass flow condition. The inlet and outlet pressure of the system together with stored soot amount were measured. Data are tabulated in table 3.1.

Table 3.1) Pressure drop for DPF during the filtration process

Mass flow	Pressure	Pressure	Soot load	Pressure drop
g/s	Pa(in)	Pa(out)	(gr)	(kpa)
38.2	107254	104027	0.6	3.226
37.6	108540	104037	1.1	4.503
37.2	110455	104050	1.8	6.405
38.0	112290	104090	2.2	8.2
37.6	114003	104083	2.7	9.92
37.9	115466	104113	3.1	11.353
37.7	116702	104107	3.6	12.595
37.8	118050	104116	4.1	13.934
37.9	119280	104129	4.5	15.151
37.8	120384	104140	5.0	16.244
37.8	121467	104140	5.4	17.327
37.8	122626	104153	5.8	18.473
37.8	123723	104153	6.2	19.57
37.8	124866	104160	6.6	20.706
37.7	125838	104166	7.0	21.672

As it is obvious, pressure drop increases as soot builds up inside the filter. The outlet flow exits as exhaust flow to the air so the outlet pressure is constant and the inlet pressure increases instead.

In tables 3.2 and 3.3 flow properties before and after filtration are listed. As it is mentioned previously FTIR and DMS apparatus were applied to detect and measure particle types and numbers.

Table 3.2) Flow properties of the inlet in different steps of soot build-up

CO2	H2O	O2	NO	NO2	Particles	Particles	Pressure	soot in filter
ppm	ppm	ppm	ppm	ppm	g/s	numbers / s	Pa	g
94824	94562	54577	61	76	0.001524	2819023135843	107254	0.6
96906	96428	51370	50	62	0.002551	4386418512334	108540	1.1
97315	96793	50741	50	58	0.002728	4874504114081	110455	1.8
95755	95396	53143	56	66	0.001899	3512399665258	112290	2.2
96454	96023	52066	56	61	0.002174	4020855180380	114003	2.7
96116	95720	52587	58	63	0.001967	3638357745407	115466	3.1
96259	95848	52367	58	63	0.002115	3911959292101	116702	3.6
96503	96067	51990	59	60	0.002330	4005817546141	118050	4.1
95718	95363	53200	59	65	0.001883	3481821044167	119280	4.5
96235	95827	52403	61	62	0.002108	3897510285335	120384	5.0
95949	95570	52845	59	65	0.001797	3323837101445	121467	5.4
96197	95792	52462	61	61	0.001941	3590097092940	122626	5.8
95974	95593	52805	59	63	0.001933	3574041022301	123723	6.2
96118	95721	52585	61	59	0.002039	3770636949968	124866	6.6
96102	95708	52608	59	62	0.001951	3607715675502	125838	7.0

Table 3.3) Flow properties of outlet in different steps of soot build-up

soot in filter	CO2	H2O	O2	NO	NO2	Particles	Particles	Pressure
g	ppm	ppm	ppm	ppm	ppm	g/s	numbers / s	Pa
0.6	94841	94562	54577	95	42	0.000000148	328506924	104027
1.1	96925	96428	51370	87	25	0.000000307	692584939	104037
1.8	97333	96793	50741	86	22	0.000000547	1093162757	104050
2.2	95771	95396	53143	89	33	0.000000664	1356046474	104090
2.7	96469	96023	52066	86	32	0.000001148	2178512270	104083
3.1	96131	95720	52587	87	34	0.000001374	2806711013	104113
3.6	96274	95848	52367	88	33	0.000001924	3827421646	104107
4.1	96518	96067	51990	88	30	0.000002581	5157805058	104116
4.5	95734	95363	53200	93	32	0.000002769	5871795829	104129
5.0	96251	95827	52403	93	29	0.000003860	8085410508	104140
5.4	95967	95570	52845	95	29	0.000004164	9088219825	104140
5.8	96214	95792	52462	96	26	0.000005008	10937939417	104153
6.2	95994	95593	52805	98	24	0.000005436	12176453916	104153
6.6	96136	95721	52585	98	21	0.000006417	14182898146	104160
7.0	96123	95708	52608	100	21	0.000006678	14966890207	104166

3.2   CFD Simulation result

3.2.1   Velocity field

In this section velocity field (vector field and velocity magnitude) of the DPF are described. Figure 3.1 shows the velocity distribution over a cut of Y plane of the filter box. The inlet cone and filter box are observed in this figure. Although flow is turbulence inside the inlet cone, it develops as laminar flow inside the inlet channels.
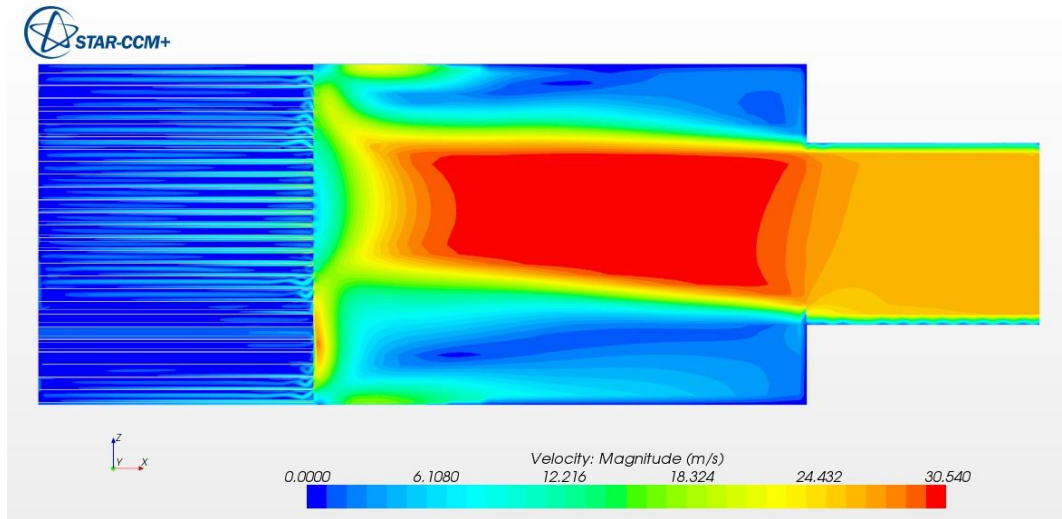
Figure 3.1) Cut of Y plane, velocity magnitude inside the inlet cone and filter box for clean filter

As it can be seen in the plot, the pipe has the effect of acceleration of velocity inside the inlet cone and it also causes non uniform distribution of the flow. At the end of the inlet cone, flow path is blocked alternatively by the outlet channels. The flow enters the inlet channels and starts developing inside the inlet channels. Two large recirculation areas near the upper and lower wall of the inlet cone are formed where the flow hits the dead end of the filter box. Flow pattern and velocity vector field are shown in Figure 3.2. Flow enters the inlet cone and accelerates in the middle of it. Turning the flow starts when it nears the filter box. As a result of turning the flow, recirculation zone forms near the entrance of the filter box. This behavior of the flow causes low efficiency for upper and lower channels of the filter box. Flow does not enter these channels effectively (Figure. 3.2)
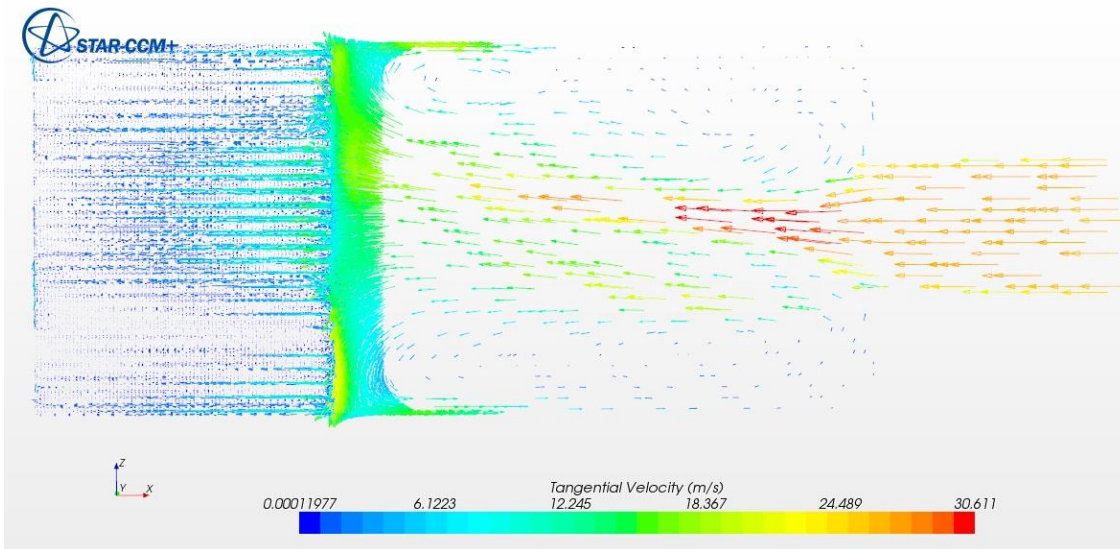
Figure 3.2) Cut of Y plane, velocity vector field inside the inlet cone and filter box for clean filter

Figure 3.3 depicts X plane cut of the filter box and outlet cone. This plot clearly shows developing the flow inside the outlet channels. Flow pattern is almost uniform and the flow regime is laminar.
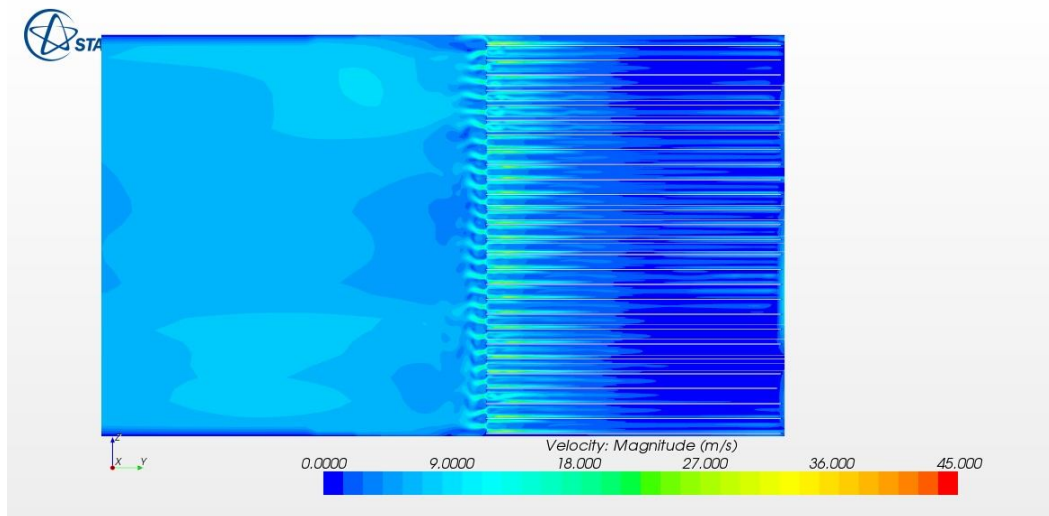
Figure 3.3) Cut of X plane, velocity magnitude inside the filter box and outlet cone for clean filter
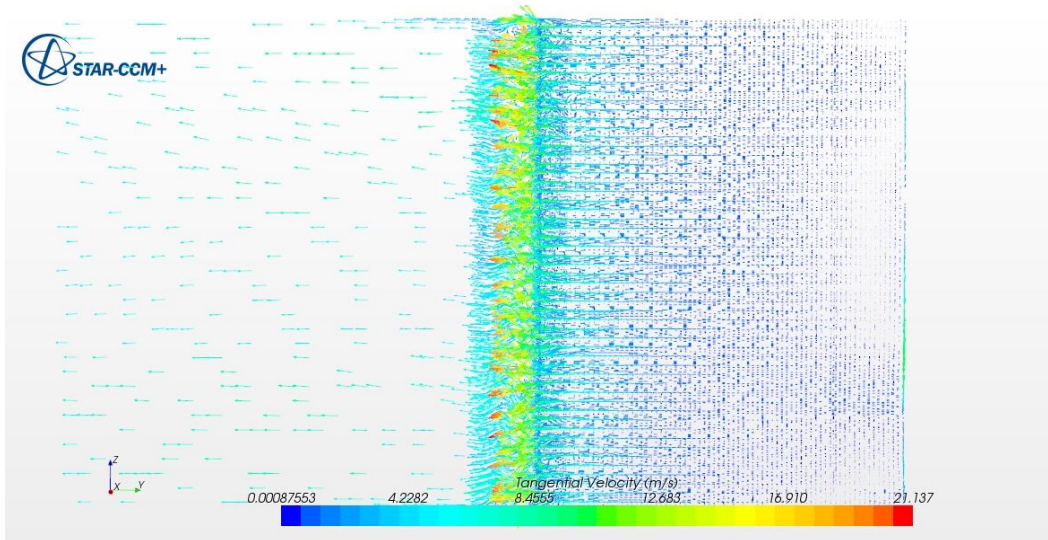
Figure 3.4) Cut of X plane, velocity vector field inside the outlet cone and filter box for clean filter

The above picture shows vector field where the flow leaves the filter box and enters the outlet cone. The flow disturbances have occurred near the connection area. There after flow moves forward smoothly. Figure 3.5 delineates zoom-in view of the connection area. Developing laminar flow inside the outlet channels is visible in this figure.

Figure 3.6 demonstrate the top view of flow pattern inside the inlet channel in the middle height of the filter box. Figure 3.7 shows the same plot inside the outlet channel. Both figures display detaching flow near none-parallel side of the inlet cone. This effect is mirrored to the other side of the symmetry boundary of the cone. Detaching flow near the wall together with the effect of pipe in acceleration causes concentration of the flow in the middle of the inlet cone. Therefore flow mainly enters the filter box in the middle. When flow passes approximately 2/3 of the filter box, it has almost crossed the upper and lower filter plates and develops inside the outlet channels. Therefore, near the end of the inlet channels, the velocity magnitude is almost zero (Figure 3.8). Moreover, Figure 3.6 represents an important behavior of flow inside the inlet channels. According to the flow pattern in this figure, exhaust flow drift towards the corner of the inlet cone and accelerates along the wall inside the inlet cone. This occurs due to the high pressure drop for air flow passing through the inlet channel. This pressure drop is dominant compared to the pressure drop of filtration for clean filter. Thus flow selects the shortest path to exit the filter box. This effect is also shown in velocity magnitude plot (Figure 3.8).
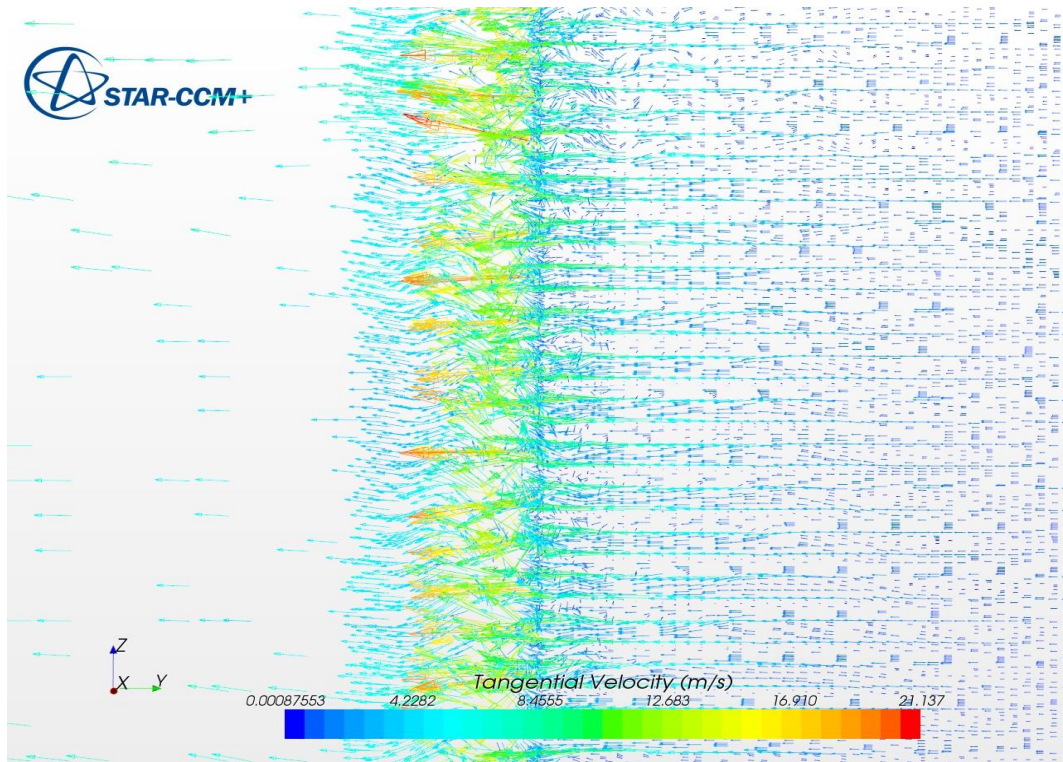
Figure 3.5) Zoom-in view of connection area; the outlet channel and outlet cone
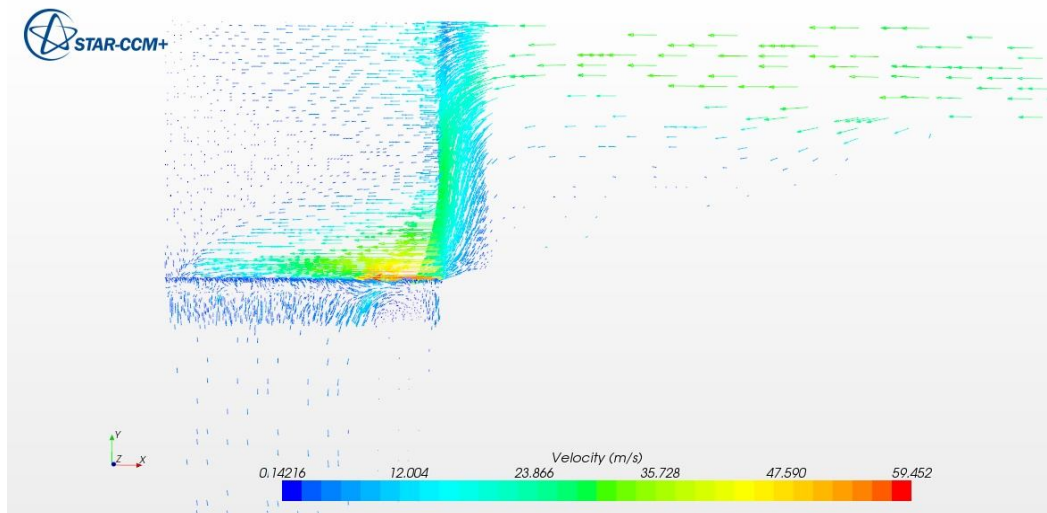
Figure 3.6) Cut of Z plane inside the inlet channel in the middle height of the filter box
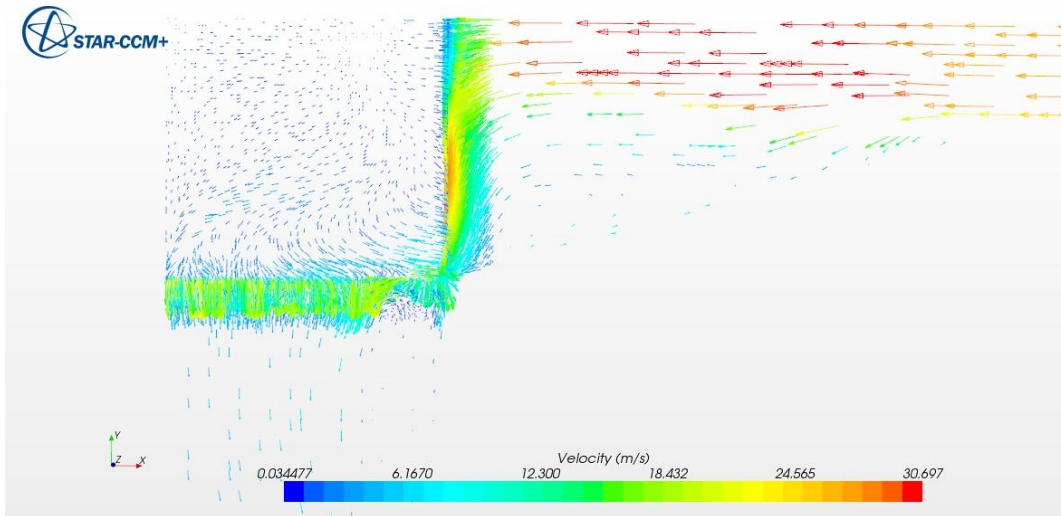
Figure 3.7) Cut of Z plane inside the outlet channel in the middle height of filter box
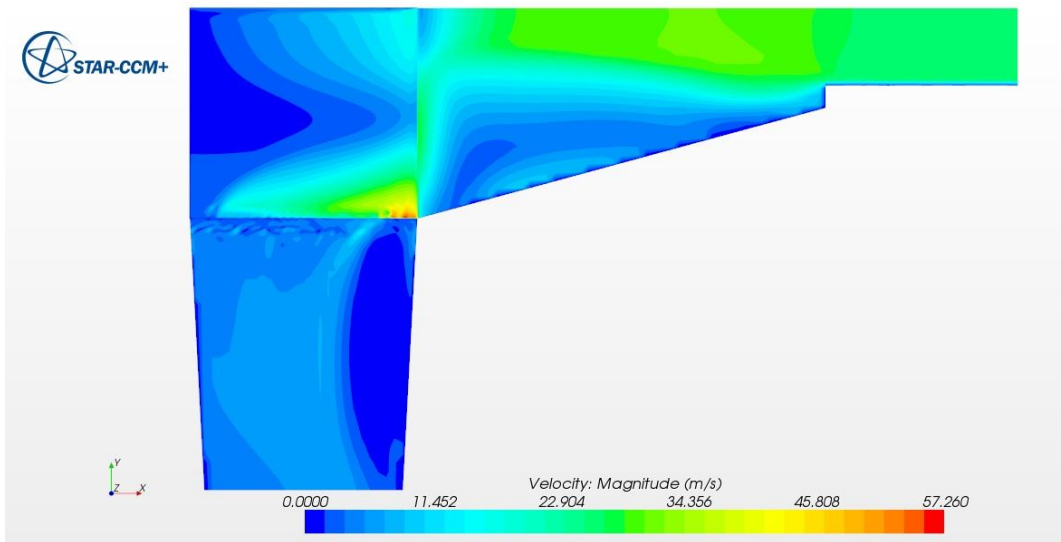
Figure 3.8) Velocity distribution inside the inlet channel, Z plan cut in the middle of the filter box

Figure 3.8 and 3.9 demonstrate the velocity distribution over a Z plane on the top and down cut of the filter box. Although the trend of the flow is the same inside the filter box, the flow of air towards the wall inside the inlet channel is more likely in the bottom and middle compared to the top of the filter box.

CHALMERS, *Applied Mechanics*, Master's Thesis 2012:57
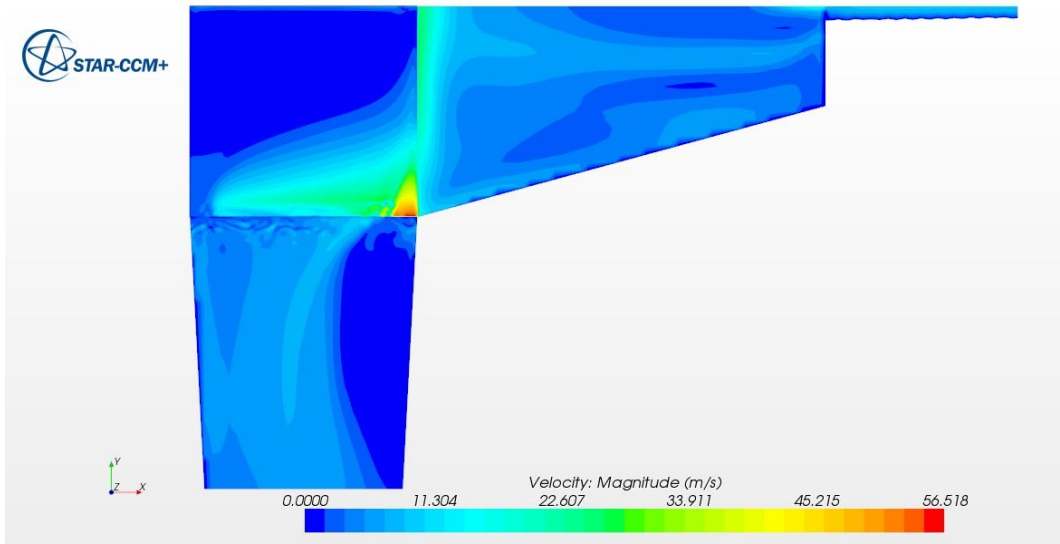
Figure 3.9) Velocity distribution inside the inlet channel, Z plan cut at the bottom of the filter box
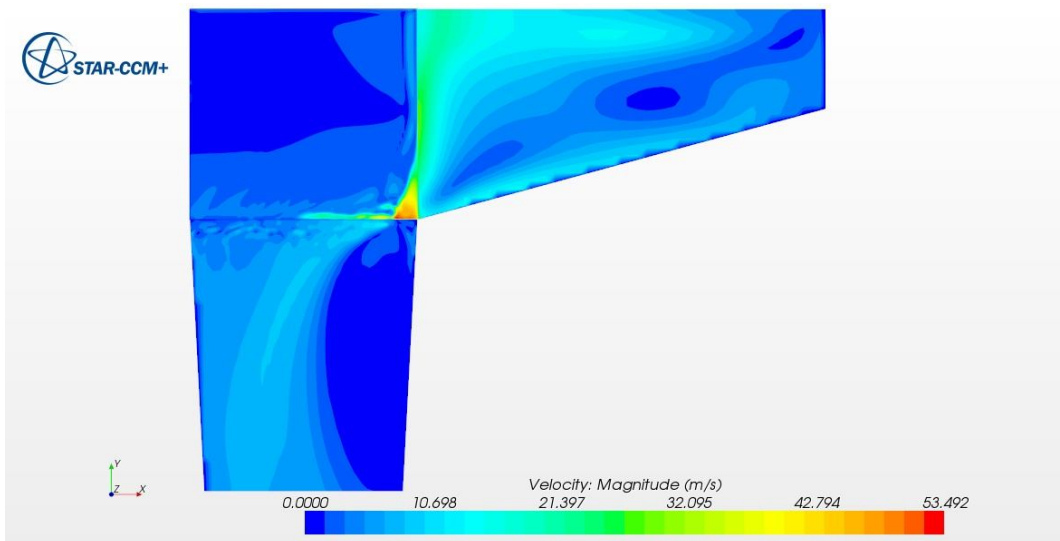
Figure 3.10) Velocity distribution inside the inlet channel, Z plan cut at the top of the filter box

All previous plots described the flow pattern and velocity distribution of clean DPF. Following figures display the DPF in three different steps of filtration by simulation of pressure drop inside the filter box. As it is described in section 1.3.3, pressure drop due to the filtration is simulated by adjusting the viscous and inertial resistance factors in equation (1.11). Since the flow through the porous media of a filter is only laminar, the second term of this equation is neglected.
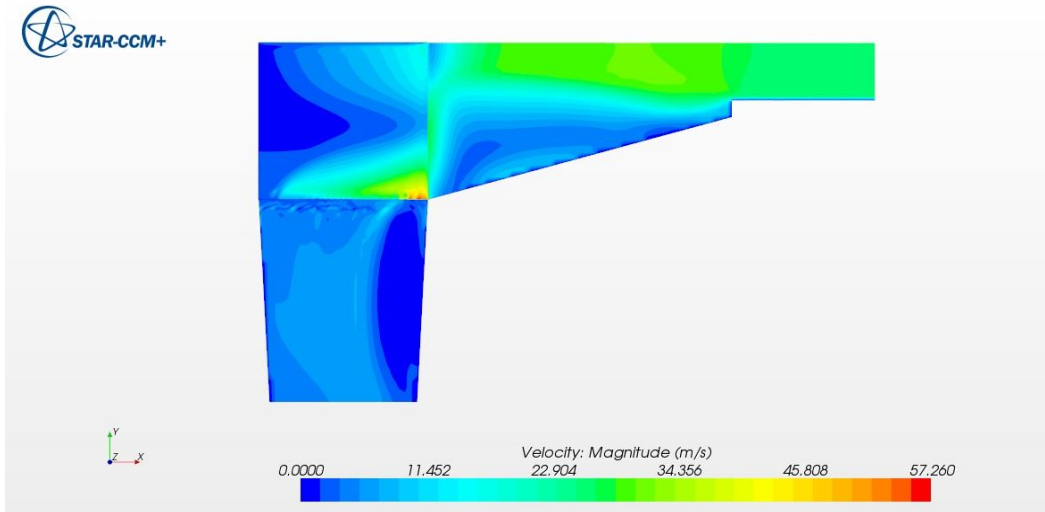
Figure 3.11) Velocity distribution over a Z plan cut of the inlet channel for clean filter (ΔP = 2.5kpa)
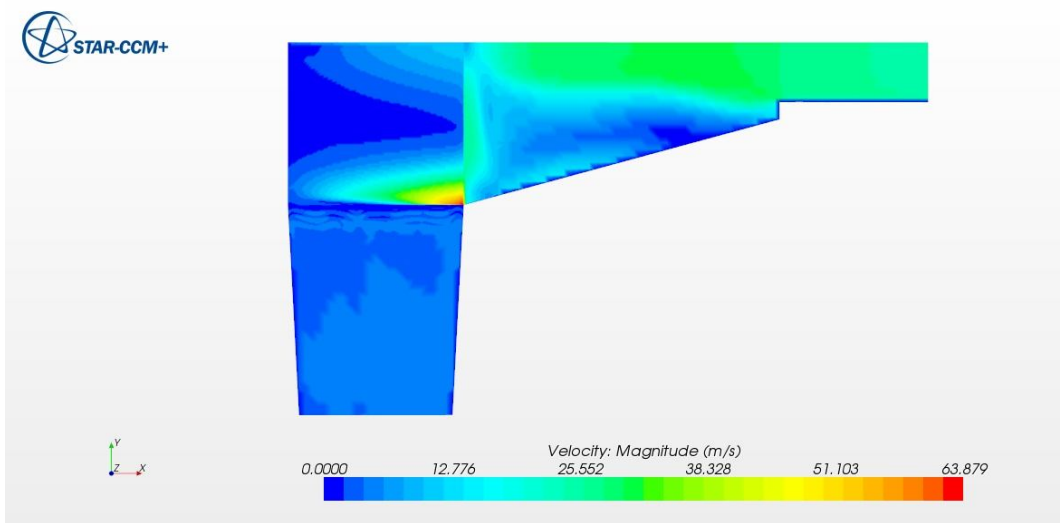
Figure 3.12) Velocity distribution over a Z plan cut of the inlet channel for semi dirty filter (ΔP = 9kpa)

Comparing Figures 3.11 to 3.14 disclose this fact: the more the pressure drop over filter plates increases, the more the flow develops uniformly through the channels. These figures also confirm the conclusion of dominant pressure drop inside the inlet channel for clean filter.

CHALMERS, *Applied Mechanics*, Master's Thesis 2012:57
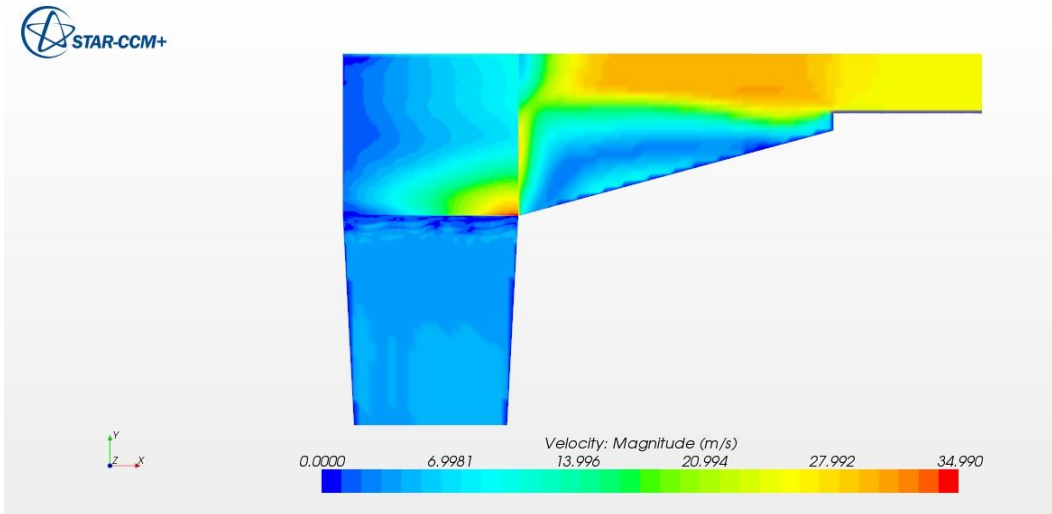
Figure 3.13) Velocity distribution over a Z plan cut of the inlet channel for semi dirty filter ($\Delta P = 13kpa$)
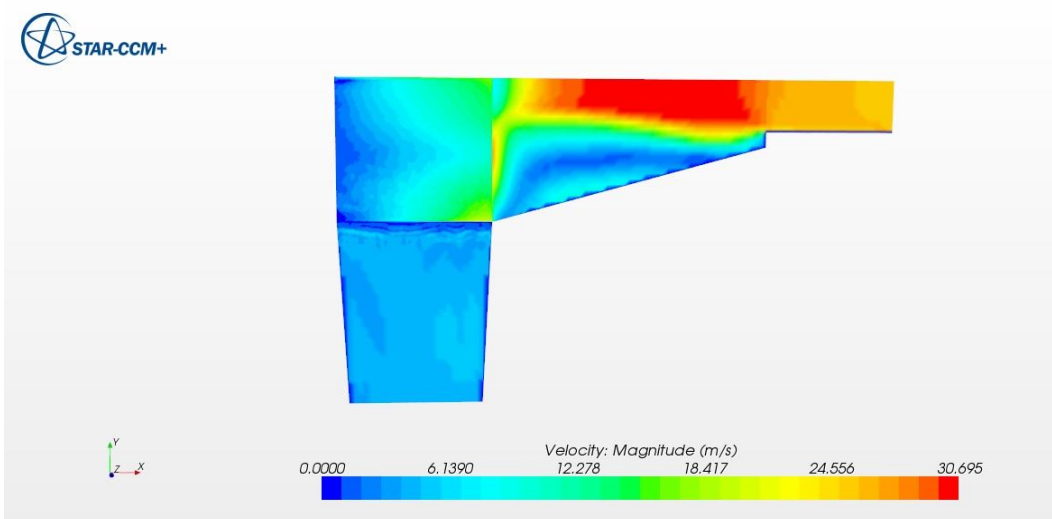
Figure 3.14) Velocity distribution over a Z plan cut of the inlet channel for dirty filter ($\Delta P = 25kpa$)

Flow distribution inside the inlet cone is not significantly affected by pressure drop inside the filter box; the difference is only in velocity range which is lower for higher pressure drop condition. Table 3.4 listed the pressure drop and viscous resistance data for different steps of soot build-up inside the DPF. These data are also compared by experimental data of the filtration process.

Table 3.4) Tuning pressure drop factor for simulation

	ΔP Exp. (kpa)	Soot amount Exp. (gr)	ΔP Sim. (kpa)	Viscous resistance coefficient
Clean filter	3.2	0.6	2.5	5000
Semi dirty 1	9.9	2.7	9	1e7
Semi dirty 2	13.9	4.5	13	1e8
Dirty filter	21.6	7.0	25	5e8

One of the objectives of this study is to investigate the possibility of soot build-up simulation over the filter plates during the filtration. Figures 3.15 to 3.17 demonstrate the velocity distribution over the same filter plate (filter no. 27 in the middle of the filter box) for clean to dirty filter. The filtration process is isothermal and flow density is constant during the filtration. Thus, mass flow distribution follows the same trend as velocity distribution. The velocity distribution over a filter plate for different steps of filtration has been illustrated in Figures 3.15 to 3.17.
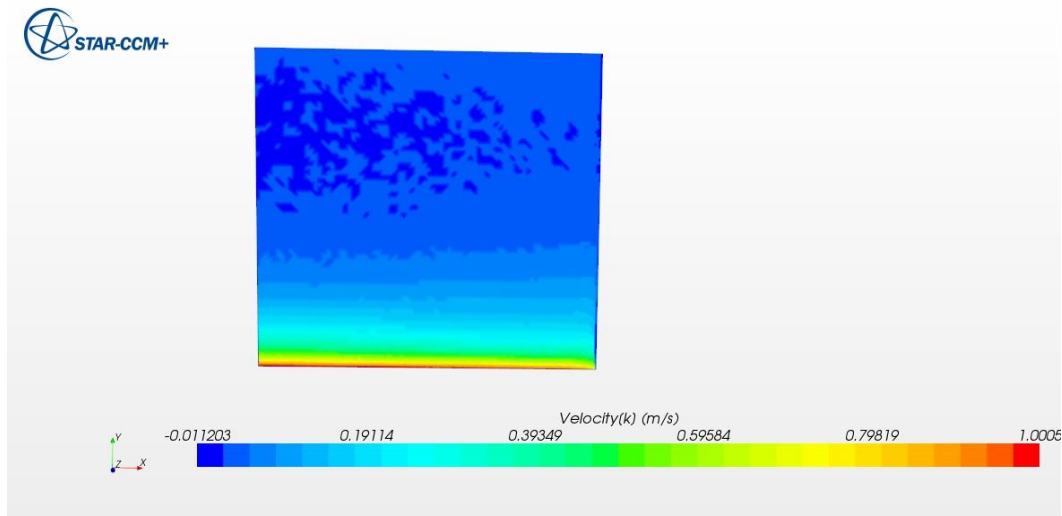
Figure 3.15) Velocity distribution over filter plate for clean filter (filter no. 27)
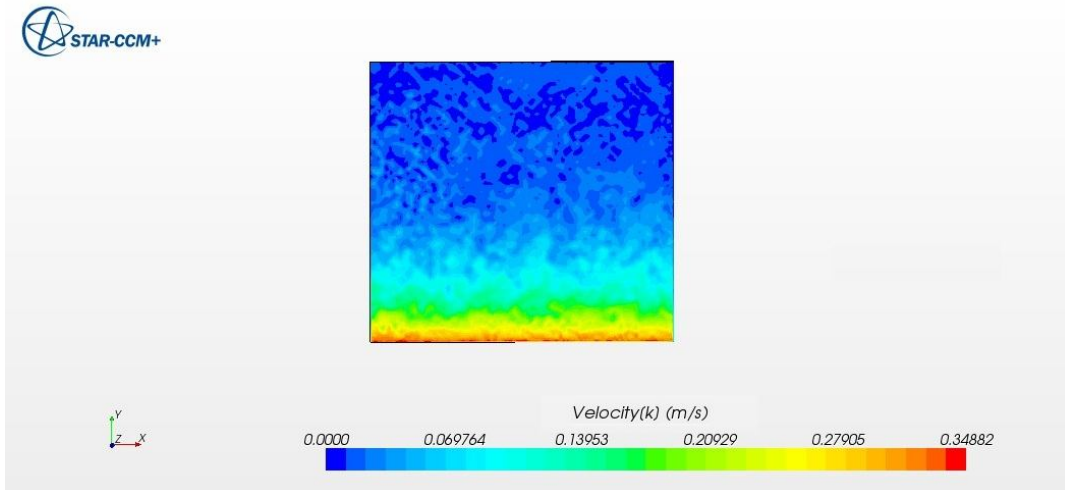
Figure 3.16) Velocity distribution over filter plate for semi dirty filter (filter no. 27)
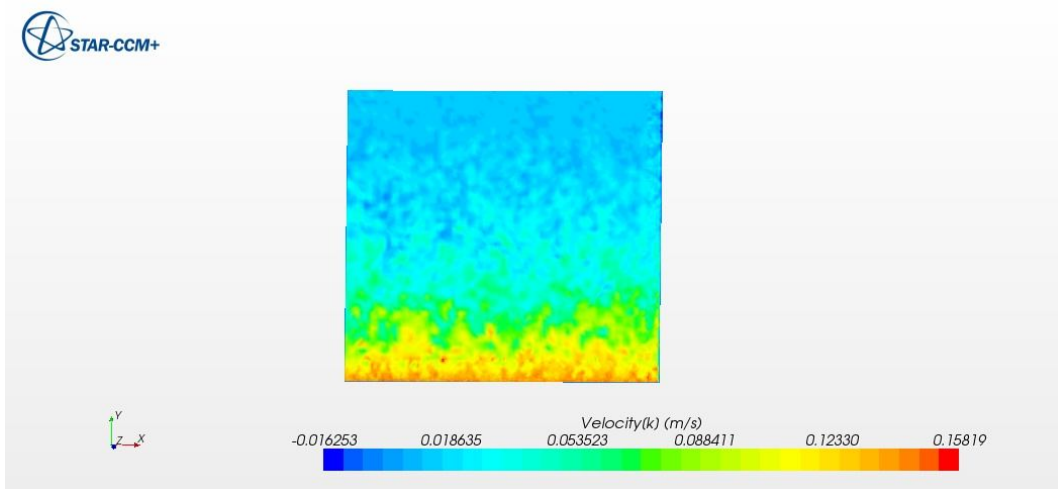
Figure 3.17) Velocity distribution over filter plate for dirty filter (filter no. 27)

Reviewing Figures 3.15 to 3.17 leads to an important conclusion regarding soot build-up simulation.

As it can be seen in these figures, the maximum amount of mass flow is observed along the side next to the outlet cone. Air flow tends to pass the filter plate in this area due to the shorter path and consequently lower pressure drop. This conclusion is reasonable for clean filter but not the semi dirty or dirty filter. During the filtration, soot is built up over the plate in this section and the pressure drop increases gradually in this area. Therefore, the low pressure drop area moves forward towards the center of the filter plate. But it is impossible to simulate this behavior in the steady state simulation. The only way to simulate the soot build-up over the filter plate is to keep the record of pressure drop for each step of filtration and then apply it as a feedback to adjust the correct site of pressure drop for the next step by a user defined correlation between pressure drop and location.

Figures 3.18 to 3.19 display velocity distribution over filter plates in different height of filter box. The difference in velocity distribution and flow profile in different heights of the filter box which is discussed in chapter 3.2.1 are obvious on filter plates.
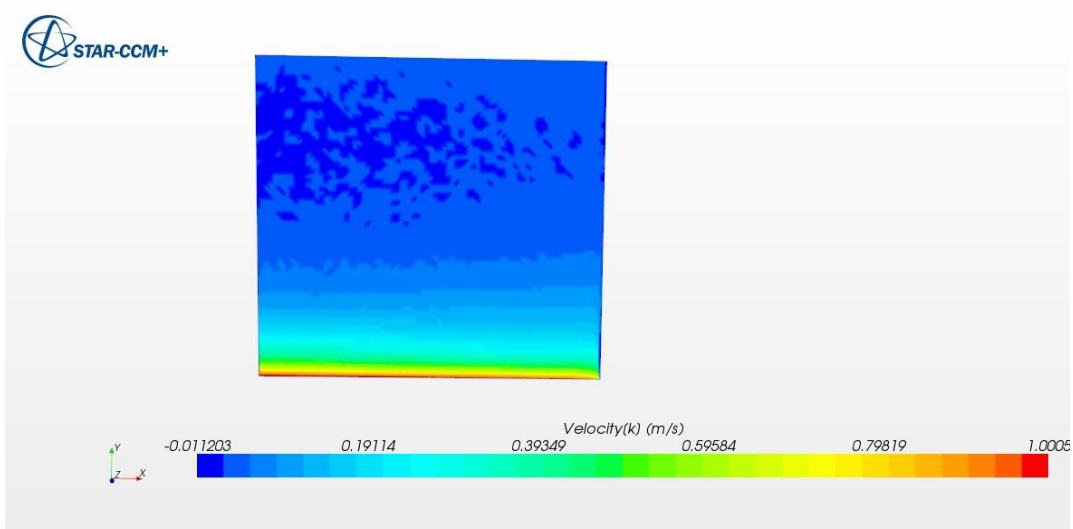

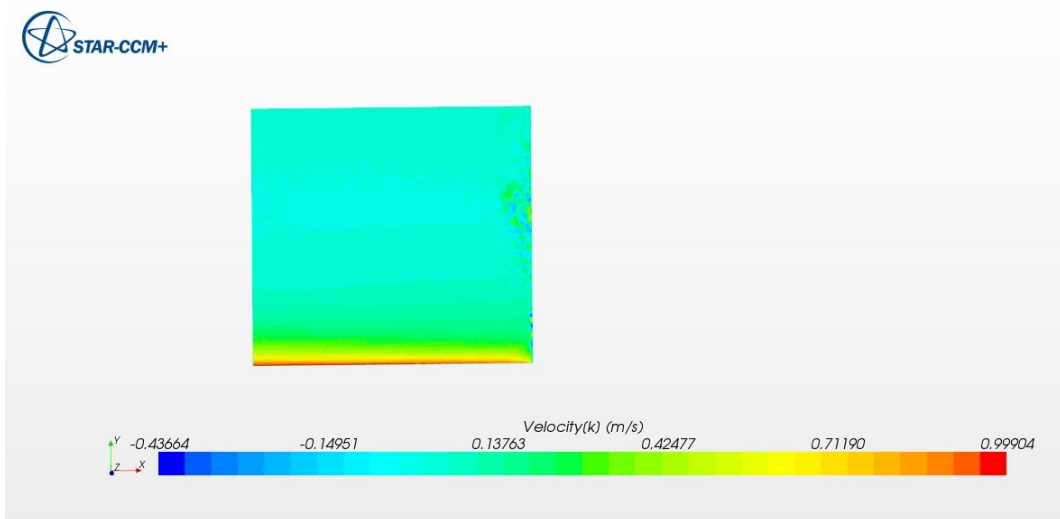*Figure 3.18) Velocity distribution over filter plate no. 3 (semi dirty filter 1)*

Figure 3.19) Velocity distribution over filter plate no.27 (semi dirty filter 1)

3.2.2 Pressure field

The overall pressure drop of the system (the outlet and inlet cone pressure difference) in each step of the filtration is listed in table 3.4. Figures 3.20 to 3.21 delineate pressure distribution of the inlet cone and inlet channel over a Z plane cut in the middle of the DPF. These results are in consistence with the velocity plot. Low pressure area is observed near the wall next to the outlet cone but the pressure increases gradually towards the center of the inlet channel.
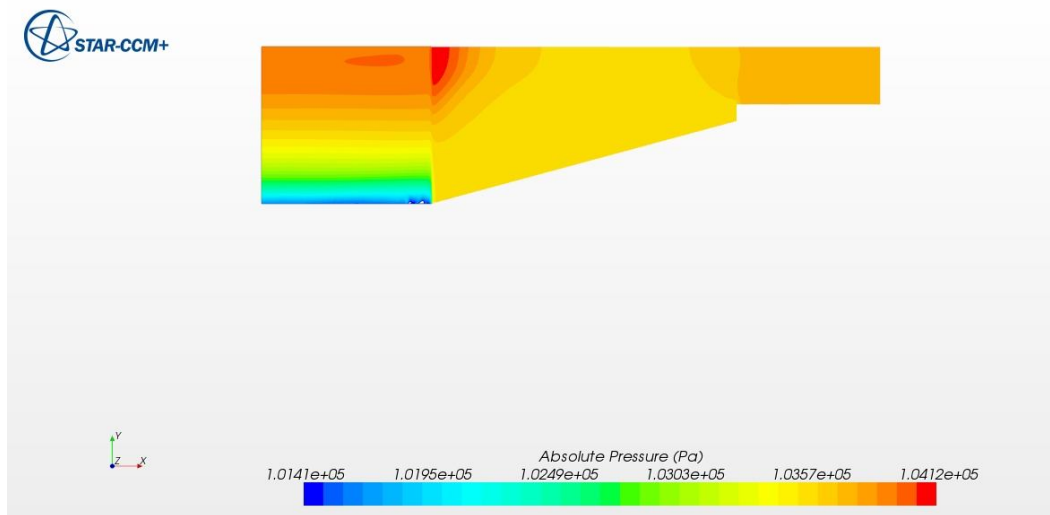
Figure 3.20) Pressure distribution for the inlet cone and inlet channel, clean filter ($\Delta P = 2.5 kpa$)
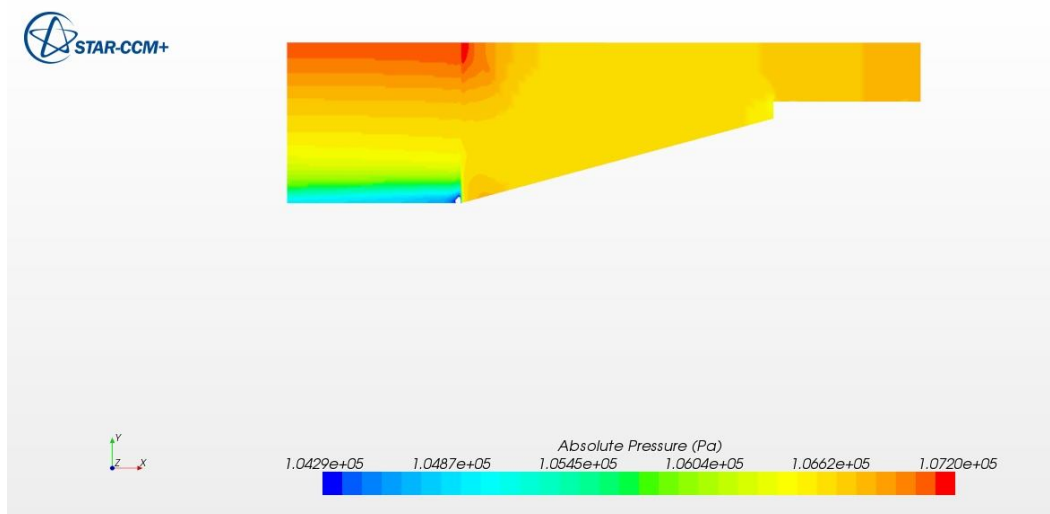
Figure 3.21) Pressure distribution for the inlet cone and inlet channel, semi dirty filter ($\Delta P = 9\ kpa$)

Maximum range of pressure distribution grows up when the soot load inside the DPF increases. (Figures 3.20 and 3.21). All figures consist of a low pressure area near the symmetry boundary where the flow enters the inlet channel. This behavior occurs due

to the change in flow direction. As it is explained in section 3.2.1 flow selects the shorter path to experience the lower pressure drop. The direction change starts near the inlet of channels especially in the middle of the inlet cone and it causes low flow velocity in this region. Consequently, high pressure magnitude is observed in this area (Figures 3.20 and 3.13).
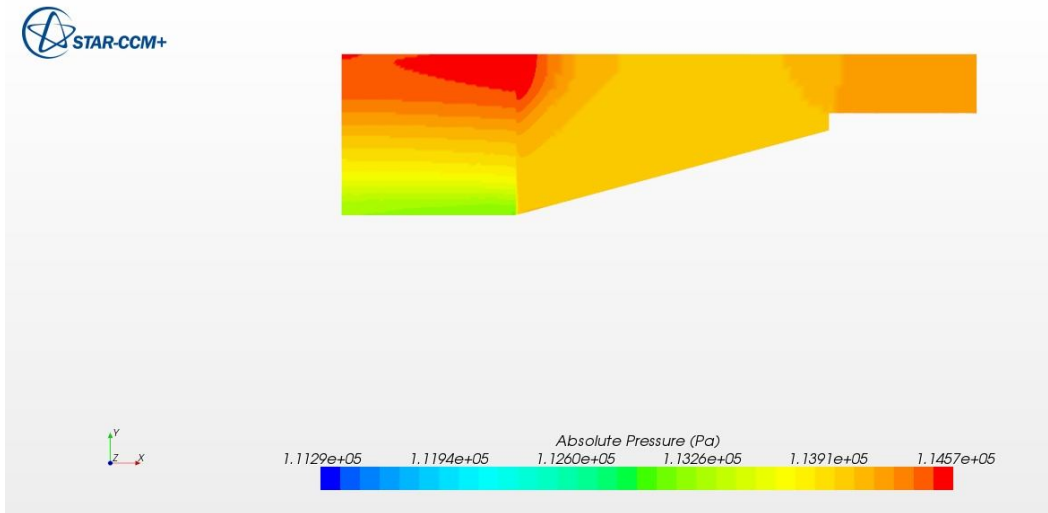

Figure 3.22) Pressure distribution for the inlet cone and inlet channel, semi dirty filter 2 (ΔP = 13 kpa)

Figure 3.23) Pressure distribution for the inlet cone and inlet channel, dirty filter (ΔP = 25 kpa)

Figures 3.24 to 3.27 depict the pressure distribution for a cut through the outlet channel in the middle of the DPF. In these figures, complete range of pressure change from inlet to outlet is observed.
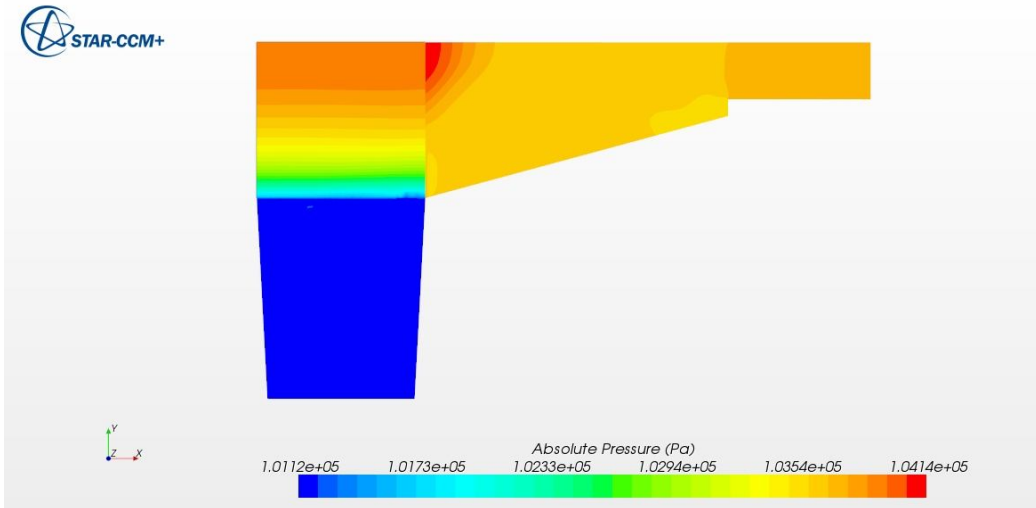
Figure 3.24) Pressure distribution over a cut through the outlet channel, clean filter ($\Delta P = 2.5\ kpa$)
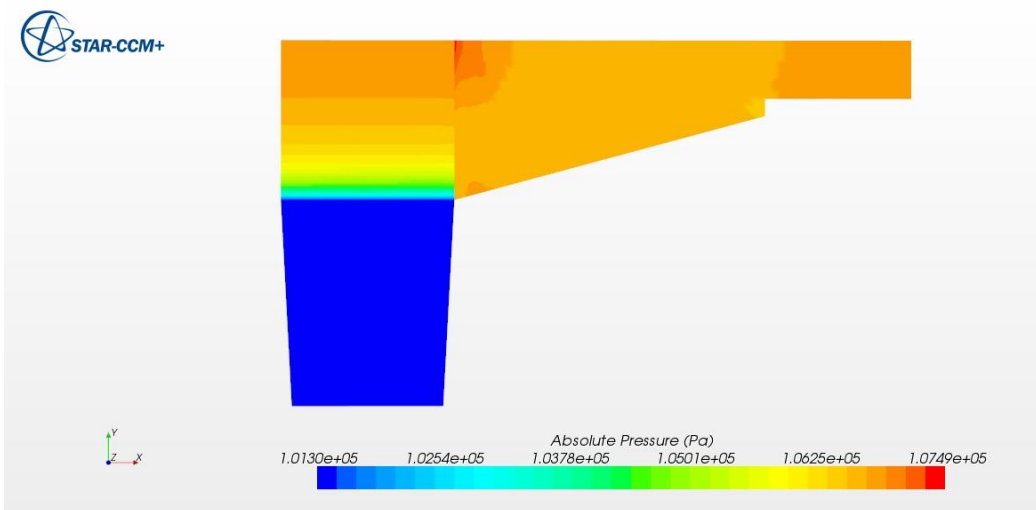

Figure 3.25) Pressure distribution over a cut through the outlet channel, semi dirty filter 1 ($\Delta P = 9\ kpa$)
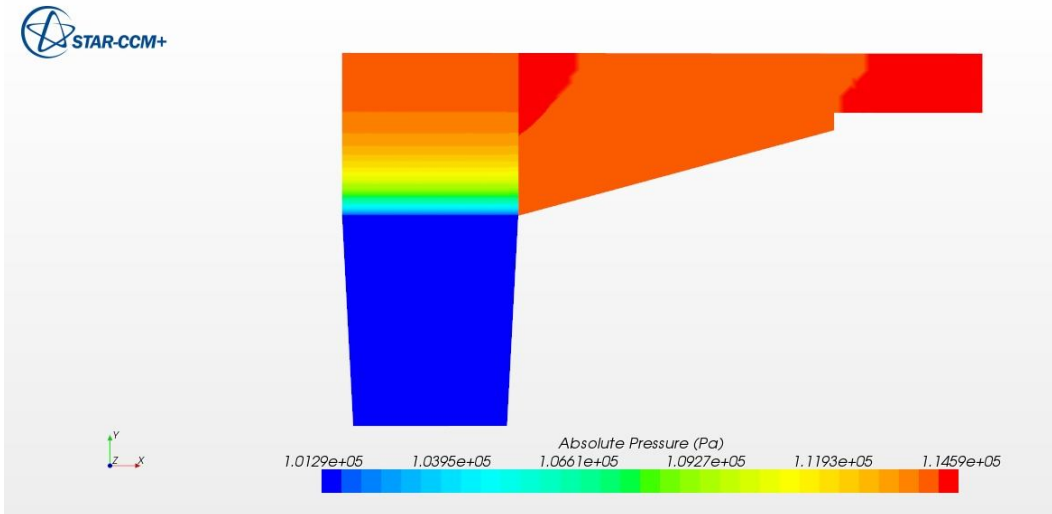
Figure 3.26) Pressure distribution over a cut through the outlet channel, semi dirty filter 2 ($\Delta P = 13\ kpa$)
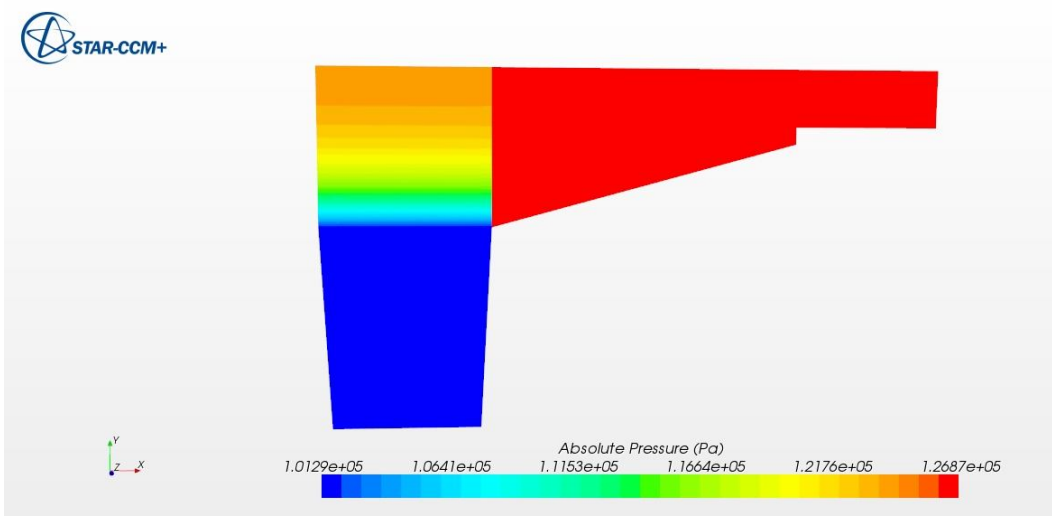

Figure 3.27) Pressure distribution over a cut through the outlet channel, dirty filter ($\Delta P = 25\ kpa$)

CHALMERS, *Applied Mechanics*, Master's Thesis 2012:57

3.2.3 DPF model with and without pipe

This section is dedicated to study of the DPF structure efficiency by comparing CDF results for the DPF CAD model with and without pipe. Figures 3.28 and 3.29 illustrate the profile of velocity magnitude for the DPF without pipe and DPF with pipe respectively.
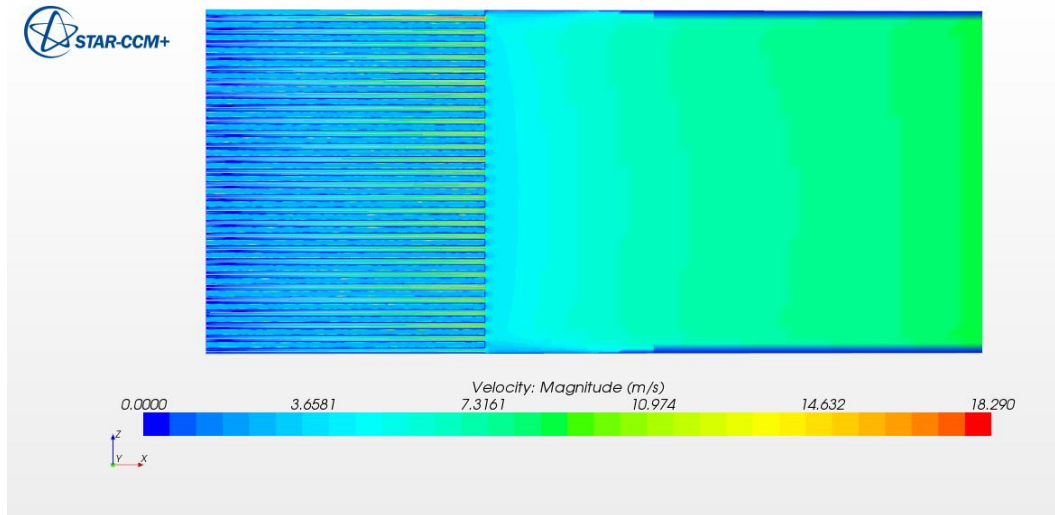

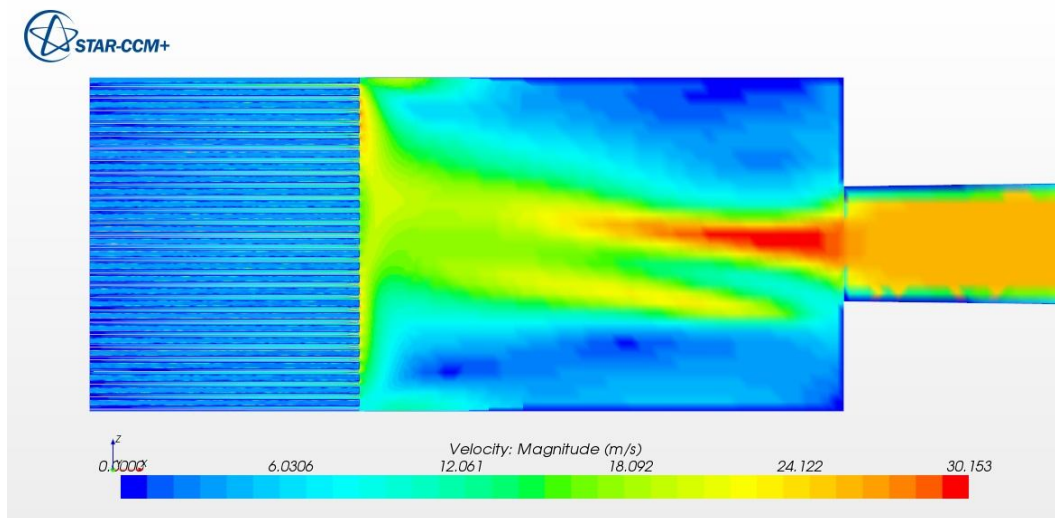*Figure 3.28) Velocity plot for the inlet cone and filter box, DPF without pipe ($\Delta P = 23\ kpa$)*

Figure 3.29) Velocity plot for the inlet cone and filter box, DPF with pipe ($\Delta P = 25\ kpa$)

Comparing these two figures demonstrates the effect of pipe on flow distribution in filtration. Apparently, the flow distributes uniformly inside the inlet cone and filter box for DPF without pipe. But presence of pipe in the second model makes a jet of flow which contributes to the acceleration of velocity in the middle of the inlet cone and consequently non-uniform flow through the filter box. Figure 3.26 displays

relatively high mass flow inside inlet channels in the middle of filter box and almost zero mass flow through lower and upper channels. This effect brings about an uneven soot build-up over the filter plates and makes upper and lower filters inefficient. This behavior might be emphasized when filter box is more packed with soot. As it was discussed previously soot build-up starts near the wall next to the outlet cone. When these areas are packed with soot, the center of the filter box is the area with low pressure drop and flow will drift into the center of the inlet channel. This fact may change when the whole filter plates in the middle are packed. Then flow starts to move upward and downward of the filter box. To summarize, the effect of pipe in DPF structure is non-homogeneous flow distribution through the inlet cone and filter box which brings about un-even soot build-up over the filter plates.

3.2.4   Residuals

Figures 3.30 and 3.31 depict normalized residuals for two samples of CFD simulations.
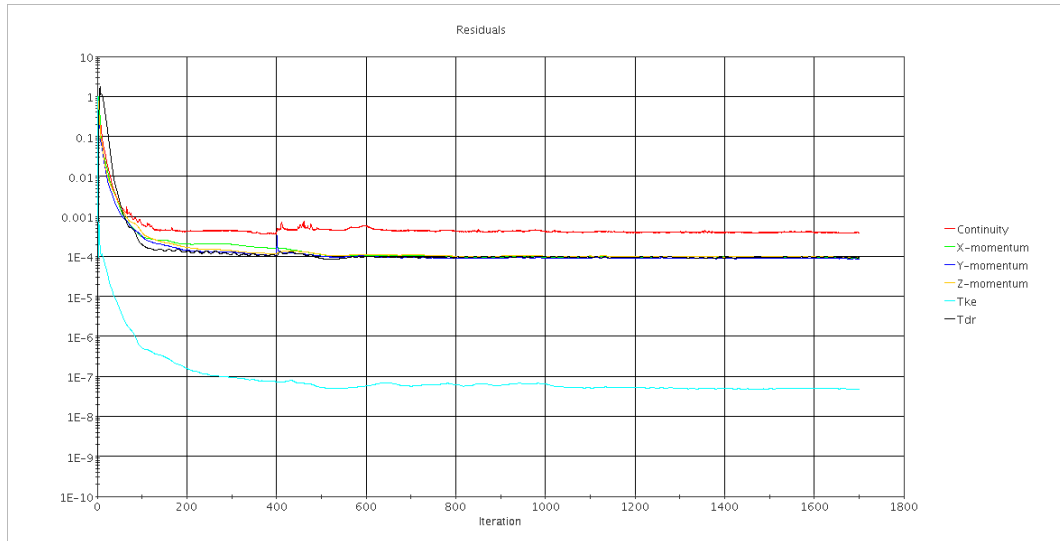

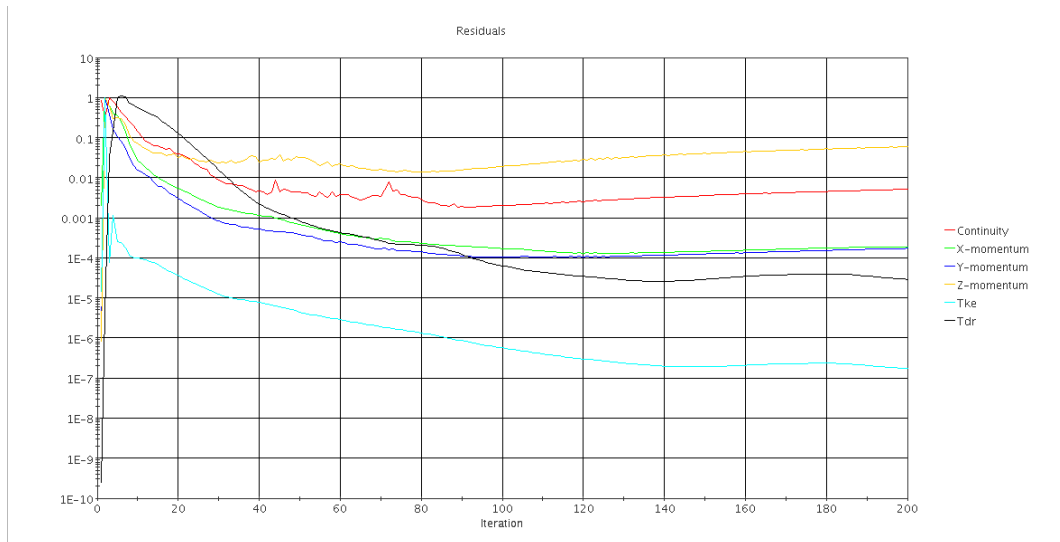*Figure 3.30) Residuals for the DPF model CFD simulation ($\Delta P = 2.5\ kpa$)*

Figure 3.31) Residuals for the DPF model CFD simulation ($\Delta P = 9\ kpa$)

4 Conclusion

Complete CAD model of Mistra DPF was prepared to investigate the flow pattern and simulate the pressure drop in different steps of filtration process. Simulation converged with satisfactory residual accuracy. The flow pattern was successfully simulated inside the DPF; through the inlet cone, all 54 inlet and outlet channels, 54 filter plates and outlet cone. Flow behavior through channels and filters was predicted correctly, for instance turning the flow direction from the inlet to outlet and passing flow through upward and downward filter plates in every single channel. The experimental data of filtration process was applied to tune the viscous resistance parameters to simulate the pressure drop in different steps of the filtration. Results for velocity distribution inside the filter box showed high pressure drop inside the inlet channel compare to the filter plates for clean filter. This effect causes non-uniformity in velocity and mass flow distribution through the channels. More uniform distribution for mass flow and velocity was observed while pressure drop increased.

Investigation of velocity distribution over the filter plates in different steps of filtration disclosed this fact that it is not possible to simulate the soot build-up over the filter plate unless the history behavior of the flow filed can be recorded. The results illustrate soot starts to cover the surface of the filter in the area next to the wall of the outlet cone. When this area is packed, the lower pressure drop area for the flow will be the center of the filter plate. Only a pressure drop-location correlation which is defined as a user defined function in the CFD tool can predict the correct location of pressure drop and consequently the soot build-up site over the filter plate.

Comparison of the flow distribution for the DPF CAD model with and without pipe demonstrated the effect of pipe on non-homogeneous flow distribution through filter box which can cause non-uniform soot build-up over the filter plates. Comparing velocity plot for these two models showed concentration of the flow through the inlet channels and filters in the middle of the filter box which makes upper and lower filters inefficient at least for the first steps of filtration. This fact might be changed when all the filter plates in the middle of filter box are packed with soot.

5   References

1. Majewski W. Addy, (2011), *Diesel particulate filter*, www.DieselNet.com,

2. Ström Henrik (2011) *Particulate Flows in After treatment Systems*, , phD thesis, Chalmers University of Technology

3. Tandon, Puskar (2010), Measurement and prediction of filtration efficiency evolution of soot loaded diesel particulate filters, , *chemical engineering science*, Vol. 65, 4751-4760

4. Torregrosa A.J., (2011), A fluid dynamic model for unsteady compressible flow in wall-flow diesel particulate filter, *Energy*, Vol. 36, 671-684

5. Ström Henrik & Andersson Bengt, (2009), Simulations of trapping of diesel and gasoline particulate matter in flow-through devices, *Top Catal.* Vol. 52, 2047-2051

6. Janoske U., (2006), Modeling of filtration and regeneration processes in diesel particulate traps*, Mathematics in Industry*, Vol. 8, 252-256

7. Versteeg H., Malalasekera W., (2007), *An introduction to computational fluid dynamic, the finite volume method*, Pearson publication, England

8. Lars Davidson,(2011), *MTF256 Turbulent flow course notes, (Division of fluid dynamic*, Applied Mechanics department, Chalmers

9. *User guide STAR-CCM+ Version 6.02.008 60.2* (2011)

10. Mistra report ER-530365, (2010), Volvo group track technology (GTT)